IOWA STATE UNIVERSITY
Digital Repository

Retrospective Theses and Dissertations

Iowa State University Capstones, Theses and Dissertations

1978

Micromechanism of wear at polymer-metal sliding interface

Malay Kumar Kar
Iowa State University

Follow this and additional works at: https://lib.dr.iastate.edu/rtd

 Part of the Mechanical Engineering Commons

Recommended Citation
Kar, Malay Kumar, "Micromechanism of wear at polymer-metal sliding interface " (1978). *Retrospective Theses and Dissertations*. 6499.
https://lib.dr.iastate.edu/rtd/6499

This Dissertation is brought to you for free and open access by the Iowa State University Capstones, Theses and Dissertations at Iowa State University Digital Repository. It has been accepted for inclusion in Retrospective Theses and Dissertations by an authorized administrator of Iowa State University Digital Repository. For more information, please contact digirep@iastate.edu.

www.manaraa.com

INFORMATION TO USERS

This material was produced from a microfilm copy of the original document. While the most advanced technological means to photograph and reproduce this document have been used, the quality is heavily dependent upon the quality of the original submitted.

The following explanation of techniques is provided to help you understand markings or patterns which may appear on this reproduction.

1. The sign or "target" for pages apparently lacking from the document photographed is "Missing Page(s)". If it was possible to obtain the missing page(s) or section, they are spliced into the film along with adjacent pages. This may have necessitated cutting thru an image and duplicating adjacent pages to insure you complete continuity.

2. When an image on the film is obliterated with a large round black mark, it is an indication that the photographer suspected that the copy may have moved during exposure and thus cause a blurred image. You will find a good image of the page in the adjacent frame.

3. When a map, drawing or chart, etc., was part of the material being photographed the photographer followed a definite method in "sectioning" the material. It is customary to begin photoing at the upper left hand corner of a large sheet and to continue photoing from left to right in equal sections with a small overlap. If necessary, sectioning is continued again — beginning below the first row and continuing on until complete.

4. The majority of users indicate that the textual content is of greatest value, however, a somewhat higher quality reproduction could be made from "photographs" if essential to the understanding of the dissertation. Silver prints of "photographs" may be ordered at additional charge by writing the Order Department, giving the catalog number, title, author and specific pages you wish reproduced.

5. PLEASE NOTE: Some pages may have indistinct print. Filmed as received.

University Microfilms International
300 North Zeeb Road
Ann Arbor, Michigan 48106 USA
St. John's Road, Tyler's Green
High Wycombe, Bucks, England HP10 8HR

7900189

KAR, MALAY KUMAR
MICROMECHANISM OF WEAR AT POLYMER-METAL SLIDING INTERFACE.

IOWA STATE UNIVERSITY, PH.D., 1978

University Microfilms International 300 N. ZEEB ROAD, ANN ARBOR, MI 48106

Micromechanism of wear at polymer-metal sliding interface

by

Malay Kumar Kar

A Dissertation Submitted to the
Graduate Faculty in Partial Fulfillment of
The Requirements for the Degree of

DOCTOR OF PHILOSOPHY

Major: Mechanical Engineering

Approved:

Signature was redacted for privacy.

In Charge of Major Work

Signature was redacted for privacy.

For the Major Department

Signature was redacted for privacy.

For the Graduate College

Iowa State University
Ames, Iowa
1978

TABLE OF CONTENTS

	Page
NOMENCLATURE	ix
1. INTRODUCTION	1
1.1. Literature Review	1
1.1.1. Mechanisms of Wear	1
1.1.2. Material Transfer	6
1.1.3. Loose Wear Fragments	8
1.1.4. Temperature Rise in Sliding and Its Effect on Wear	9
1.2. Objective and Approach to the Problem	13
2. ANALYTICAL METHODS	17
2.1. Formulation of the Heat Transfer Model	17
2.2. Heat Transfer Equation for the Rotating Disc	19
2.3. Boundary Conditions	22
2.4. Heat Distribution Coefficient	29
2.5. Heat Transfer Coefficients	32
3. EXPERIMENTAL PROCEDURE	35
3.1. Sliding Experiments	35
3.1.1. Experimental Set-Up	35
3.1.2. Temperature Measurements	37
3.2. Material Selection	39
3.3. Specimen Preparation for Sliding Experiments	40

	Page
3.4. Differential Thermal Analysis (DTA) Measurements	41
3.5. Surface Examination	42
3.5.1. Scanning Electron Microscopy	42
3.5.2. Transmission Electron Microscopy	42
3.6. Measurement of Wear Particle Size	44
4. TEST RESULTS AND DISCUSSION	45
4.1. Temperature Rise at the Disc Rubbing Surface	45
4.1.1. Measured Temperature Rise	45
4.1.2. Estimation of Heat Transfer Coefficients	52
4.1.3. Calculation of Temperature Rise	58
4.1.4. Comparison of the Measured and Predicted Temperature Rise	59
4.2. Investigation of Polymer Sliding Surface Using DTA	59
4.3. Examination of Polymer Sliding Surfaces by Scanning and Transmission Electron Microscopy	66
4.3.1. Scanning Electron Microscopy	66
4.3.2. Transmission Electron Microscopy	71
4.4. Wear Particle Analysis	81
4.4.1. Measurement of Particle Size	81
4.4.2. Estimation of Wear Particle Thickness	81
4.5. The Wear Model for Polymer-Metal Sliding	91
4.5.1. Mechanism of Wear at Low Sliding Speeds	91
4.5.2. Mechanism of Wear at Medium Sliding Speeds	91
4.5.3. Wear Failure at High Sliding Speeds	93
5. CONCLUSIONS AND SUGGESTIONS	95
5.1. Conclusions	95
5.2. Suggestions for Future Work	97

		Page
6.	ACKNOWLEDGMENTS	99
7.	REFERENCES	101
8.	APPENDIX A: COMPUTER EVALUATION	109
9.	APPENDIX B: ERROR ANALYSIS	112
10.	APPENDIX C: CALCULATION OF INTERPLANAR DISTANCES AND DIFFRACTING PLANES	114

LIST OF FIGURES

		Page
Fig. 1.	Stages showing the formation of a roll during sliding in the direction of arrow under load N.	3
Fig. 2.	Schematic representation of pin-and disc sliding system; (a) both disc and pin stationary with coordinates (r,θ) fixed to the disc, (b) rotating disc and stationary pin with coordinates (r,ψ) in reference to the pin.	18
Fig. 3.	Schematic of pin-and-disc machine showing (a) the sliding system; (b) the details of slip ring and brush arrangement for temperature measurement.	36
Fig. 4.	Schematic diagram of temperature measuring system.	38
Fig. 5.	Sketch of polymer disc showing the abrasion marks, wear tracks and replicated areas.	43
Fig. 6.	Plot of temperature vs. time for high density polyethylene (a) steady state conditions, (b) transition from steady state to unsteady state. x indicates the point of failure.	46
Fig. 7.	Plot of temperature vs. time for polyoxymethylene; (a) steady state conditions, (b) transition from steady state to unsteady state. x indicates the point of failure.	47
Fig. 8.	Plot of temperature vs. time for PTFE; (a) steady state conditions, (b) transition from steady state to unsteady state. x indicates the point of failure.	48
Fig. 9.	Plot of temperature vs. time for polypropylene under steady state conditions.	49
Fig. 10.	Plot of coefficient of friction vs. time for high density polyethylene. Curve A for 1150 g load and 0.5 m/sec speed, and curve B for 1150 g load and 2.5 m/sec speed.	51
Fig. 11.	Plots of temperature rise vs. Nusselt number with and without the Grashof number.	53
Fig. 12.	Plots of temperature rise vs. Nusselt number with and without the Grashof number.	56
Fig. 13.	Variation of $\frac{0.11Ka(0.5\ Pr)^{0.35}}{\nu^{0.7}}$ and $\frac{0.4\ Ka}{\nu^{0.5}}$ with temperature.	57

		Page
Fig. 14.	Temperature rise vs. sliding speed for high density polyethylene pin-steel disc rubbing surface in steady state condition.	60
Fig. 15.	Temperature rise vs. sliding speed for polyoxymethylene pin-steel disc rubbing surface in steady state condition.	61
Fig. 16.	Temperature rise vs. sliding speed for PTFE pin-steel disc rubbing surface in steady state condition.	62
Fig. 17.	Temperature rise vs. sliding speed for polypropylene pin-steel disc rubbing surface in steady state condition.	63
Fig. 18.	Scanning electron micrographs of polymer sliding surfaces: (a) high density polyethylene; (b) polyoxymethylene; (c) PTFE. Sliding conditions: speed 1.5 m/sec, load 2750 g. The direction of sliding is shown by the arrow.	68
Fig. 19.	Scanning electron micrographs of polymer sliding surfaces showing localized flow of material in the direction of sliding (shown by the arrow): (a) high density polyethylene; (b) polyoxymethylene. Sliding conditions: speed 2.5 m/sec, load 2750 g.	69
Fig. 20.	Scanning electron micrographs of polymer sliding surfaces: (a) high density polyethylene; (b) polyoxymethylene. Sliding conditions: speed 4 m/sec, load 2750 g. The sliding direction is shown by the arrow.	69
Fig. 21.	Scanning electron micrograph of polyoxymethylene sliding surface showing the flow of material in the direction of sliding (shown by the arrow). Sliding conditions: Same as in Fig. 20.	70
Fig. 22.	Scanning electron micrographs of PTFE sliding surface. Sliding conditions: (a) speed 2.5 m/sec, load 2750 g; (b) speed 4 m/sec, load 2750 g. The sliding direction is shown by the arrow.	70
Fig. 23.	Transmission electron micrograph of PTFE sliding surface and electron diffraction pattern from the encircled portion in the top left corner. Sliding conditions: speed 0.002 m/sec, load 1600 g, time 20 min.	72

		Page
Fig. 24.	Transmission electron micrograph of the same sliding surface as in Fig. 23, but from a different location.	73
Fig. 25.	Transmission electron micrograph of high density polyethylene sliding surface and electron diffraction pattern from the encircled portion in the top-left corner. Sliding conditions: Same as in Fig. 23.	75
Fig. 26.	Transmission electron micrograph of polyoxymethylene sliding surface and electron diffraction pattern from the encircled portion in the top-left corner. Sliding conditions: Same as in Fig. 23.	76
Fig. 27.	Transmission electron micrograph of polypropylene sliding surface and electron diffraction pattern from the encircled portion in the top-left corner. Sliding conditions: Same as in Fig. 23.	77
Fig. 28.	Transmission electron micrograph of polycarbonate sliding surface showing fragmented films and electron diffraction pattern from one such film in the top-left corner. Sliding conditions: Same as in Figure 23.	80
Fig. 29.	Histogram of wear particle area for high density polyethylene. Sliding conditions: speed 0.5 m/sec, time 1 hr.	82
Fig. 30.	Histogram of wear particle area for polyoxymethylene Sliding conditions: Same as in Fig. 29.	82
Fig. 31.	Histogram of wear particle area for PTFE. Sliding conditions: Same as in Fig. 29.	83
Fig. 32.	Histogram of wear particle area for polypropylene. Sliding conditions: Same as in Fig. 29.	83
Fig. 33.	Schematic illustration of the model for wear particle formation; (a) adhesive junction due to contact between two asperities; (b) shape of a potential wear particle at X in loaded condition; (c) shape of the wear particle due to recovery of junction in (b).	85
Fig. 34.	Schematic of the proposed wear model; (a) crystalline polymers (b) amorphous polymers.	92

LIST OF TABLES

		Page
Table 1.	DTA results for high density polyethylene sliding surfaces.	65
Table 2.	DTA results for polyoxymethylene sliding surfaces.	65
Table 3.	DTA results for PTFE sliding surfaces.	65
Table 4.	Surface area range for polymer wear particles.	84
Table 5.	Estimated thickness of polymer wear particles.	90
Table A1.	Computer evaluation of the modified Bessel function of the first kind, $I_n(\sigma R)$ (in this program a value of R = 0.51 has been used).	109
Table A2.	Computer evaluation of the modified Bessel function of the second kind, $K_n(\sigma R)$ (in this program a value of R = 0.51 has been used).	111
Table C1.	Interplanar distances and diffracting planes.	115

NOMENCLATURE

A = major axis of particle, cm

A_o = apparent area of heat generation, cm^2

A_s = surface area of flattened ellipsoid, cm^2

A' = peripheral area of the disc, cm^2

B = minor axis of particle, cm

C = thickness of transferred wear particle, Å

C_l = thickness of loose wear particle, Å

C_p = specific heat at constant pressure, cal/gm^oC

D_d = diameter of the disc, cm

d = diameter of the pin, cm

d_l = diameter of wear particle, μm

E = Young's modulus of elasticity, kg/cm^2, $dyne/cm^2$

E_a = adhesional energy, erg

E_e = elastic strain energy, erg

E_s = total surface energy, erg

Gr = Grashof Number $\left(\frac{\beta g \Delta t D_d^3}{\nu^2}\right)$

g = acceleration due to gravity, cm/sec^2

H = Brinnell hardness, kg/mm^2

h = film heat transfer coefficient for edge of the disc, $cal/sec\ cm^2\ ^oC$

h' = film heat transfer coefficient for the side of the disc, $cal/sec\ cm^2\ ^oC$

h_l = surface heat transfer coefficient for the pin, $cal/sec\ cm^2\ ^oC$

J = mechanical equivalent of heat, ergs/cal

K = proportionality constant; wear factor

k_a = thermal conductivity of air, $cal/sec\ cm\ ^oC$

k_d = thermal conductivity of the disc material, cal/sec cm ^{o}C

k_p = thermal conductivity of the pin material, cal/sec cm ^{o}C

L = characteristic length, cm

L_1 = sliding distance, cm

ℓ = length of the pin, cm

N = normal load, g

N_1 = characteristic number $\left\{\left(\frac{h_1 p}{k_p \cdot A_o}\right) 1/2\ell\right\}$

Nu = Nusselt Number $\left(\frac{hD_d}{k_a}\right)$

P = nominal contact pressure, kg/cm^2

p_o = normal pressure, kg/cm^2

p_1 = perimeter, cm

Pr = Prandtl Number $\left(\frac{\mu_v C_p}{k_a}\right)$

q = heat generated per second, cal/sec

R = radius of the disc, cm

R_1 = inside radius of the annulus, cm

Re = Reynolds number $\left(\frac{VD_d}{\nu}\right)$

r = radial coordinate

s = shear stress, kg/cm^2

T = temperature rise, ^{o}C

T_D = average temperature rise at the disc rubbing surface, ^{o}C

T_p = average temperature rise at the pin rubbing surface, ^{o}C

t = thickness of the disc, cm

t_f = ambient temperature, ^{o}C

t_s = amplitude of surface temperature, ^{o}C

t_1 = temperature at depth x, ^{o}C

Δt = temperature difference, ^{o}C

V = sliding speed, cm/sec

V_p = volume of flattened ellipsoid, cm^3

v = volume of wear, cm^3

W_{ab} = work of adhesion, erg/cm^2

w = weight loss, g

x = depth of penetration of temperature oscillation, cm

α = thermal diffusivity, cm^2/sec

α_1 = a constant

β = coefficient of thermal expansion, $1/^oC$

γ = surface energy, erg/cm^2

γ_1 = heat distribution coefficient

ϵ = Poisson's ratio

θ = angular coordinate fixed to the disc

λ_1 = wave length, cm

μ = coefficient of friction

μ_v = absolute viscosity, g/cm-sec

ν = kinematic viscosity, cm^2/sec

ρ = density, g/cm^3

σ_Y = yield strength, $dyne/cm^2$

τ = time, sec

τ_o = period of disc rotation, sec

ψ = angular coordinate with respect to heat source

Ω = contact angle, rad

ω = angular speed, rad/sec

1. INTRODUCTION

1.1. Literature Review

1.1.1. Mechanisms of Wear

The understanding of the mechanisms governing the wear of polymers sliding against metal surfaces is important from both scientific and technological standpoints. This is especially true since polymeric materials are being used more and more in sliding applications, such as bearings, friction blocks and brake devices.

Four basic mechanisms of wear are commonly recognized: adhesive, abrasive, corrosive, and wear from surface fatigue. Of these adhesive and abrasive wear mechanisms have often been used to explain the wear of polymeric materials. Adhesive wear arises from the fracture of adhesively-bonded junctions that occurs because of the relative motion between the mating surfaces. Rabinowicz and Tabor (1) studied the mechanism of adhesive-wear particle formation for several sliding metallic pairs. Burwell and Strang (2) and Archard (3) developed identical expressions for wear volume in an adhesive process. Archard and Hirst (4) studied adhesive wear for polymer-metal pairs and pointed out that the wear equation derived earlier by Archard (3) could be applied to these pairs too. Belyi et al. (5) noted that the transfer of materials is the most important characteristic of adhesive wear in polymers. The abrasive wear is produced as a result of deformation or ploughing of the softer polymer by harder asperities on the mating surface. This type of wear has been studied in detail by a number of workers (6-10). The corrosive wear is due to thermal or thermo-oxidative degradation of polymers and the resulting formation of highly reactive, low molecular weight compounds

(11). The fatigue wear is usually thought to occur during rolling, but localized fatigue on an asperity scale has now also been recognized as an important factor in sliding.(12).

In addition to the above mechanisms, Aharoni (13) proposed roll formation. According to his model, wear takes place by adhesion in the contact zone as shown in Figure 1(a) which results in the formation of a roll (b to d) that is sheared as sliding continues. Since the process of roll formation depends upon adhesion, it is no different from the basic mechanism of adhesive wear.

Suh (14) proposed the delamination theory, which assumes that the wear of metals is caused by subsurface deformation followed by crack nucleation and crack propagation. Using this concept, Suh and coworkers (14, 15) derived two equations for wear. One of these is based on the assumption that a strong junction is formed at some fraction of asperity contacts. Sliding causes the junction to be sheared, producing a wear sheet created solely as a result of the interaction of one set of asperities. The second equation is derived from the assumption that the creation of a wear sheet is a cumulative process which results when the metal is sheared a small amount by each passing asperity. The creation of a wear sheet will only occur, however, after a large number of asperities have passed over each point on the surface. The reduced form of these equations is quite similar to that of Archard's equation.

The lack of understanding of these basic mechanisms, together with the interplay of these mechanisms in any real situation, is probably responsible for the diverse correlations of wear with different material properties. For example, the abrasive wear of polymers has been shown by

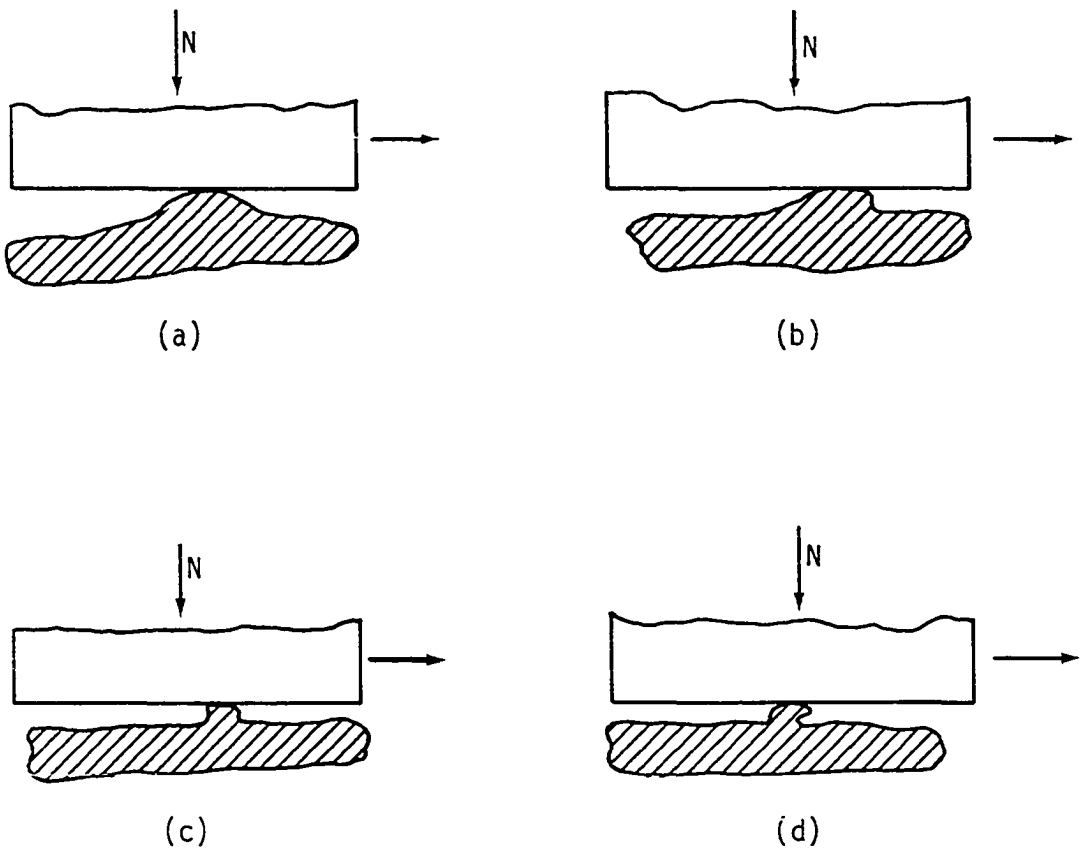

Fig. 1. Stages showing the formation of a roll during sliding in the direction of arrow under load N.

Ratner (6) to be inversely proportional to the product of the nominal fracture stress and the strain-at-fracture. Giltrow (16) showed that the abrasive wear of thermoplastic polymers varies inversely as the square root of their cohesive energy. Lontz and Kumnick (17) found that the wear rate of polytetrafluoroethylene[1] was directly proportional to the flexure modulus and inversely proportional to the yield strain. Warren and Eiss (18) have recently shown that the wear of poly(vinyl chloride) and polychlorotrifluoroethylene is inversely proportional to their energy-to-rupture.

Lancaster (10) found that for an amorphous polymer like poly(methyl methacrylate), the abrasive wear rate is a minimum near the glass transition temperature. For crystalline polymers, such as polyamides and PTFE, the change in wear rate with temperature is less marked than for the amorphous polymers until near the crystalline melting point. At this temperature, the mobility of polymer molecules increases so that the material softens, the strength decreases, and the abrasive wear rate increases.

On the basis of his model for adhesive wear, Archard (3) derived the following equation:

$$v = \frac{KNL_1}{H} \qquad (1)$$

where v is the volume of wear; H, the Brinell hardness of the softer material; L_1, the sliding distance; N, the normal load; and K, a constant which implies the probability of producing a wear particle per asperity encounter. The experimental values of K fall in the range 10^{-3} to 10^{-8}.

[1]Abbreviated as PTFE.

The above equation, though originally proposed for metals, has also been used for polymers. It involves "hardness" as a material property, which is deceptive for polymeric materials because of the occurrence of creep under ambient conditions.

Several workers have tried to express the wear of polymers in terms of the sliding variables. For example, Lewis (19) suggested the following empirical relationship for adhesive wear:

$$v = KNV\tau \tag{2}$$

where v is the volume of material worn; N, the normal load; V, the speed; τ, the time of sliding; and K, a proportionality constant called the wear factor.

Working with automotive brake linings and metal drums, Rhee (20) found that the wear rate did not vary linearly with the nominal contact pressure (P), sliding speed (V), or the time of sliding (τ), in contrast to the expression proposed by Archard (3). He therefore suggested the following empirical relationship:

$$w = KP^{a}V^{b}\tau^{c} \tag{3}$$

where w is the weight loss due to wear, and the values of the exponents, a, b, and c, depend upon the sliding pair combination. The equation was verified experimentally for polymer-bonded automotive friction materials sliding against cast iron and chromium drum surfaces. The work of Pogosian and Lambarian (21) also supports a relationship of this type for asbestos-reinforced friction materials sliding against cast iron and steel surfaces.

Kar and Bahadur (22) developed the following equation for adhesive wear volume from dimensional analysis, and the experimental wear data for

unfilled and PTFE-filled polyoxymethylene sliding against a steel surface:

$$v = 1.5 \frac{K\gamma^{1.775} P^{1.47} L_1^{1.25}}{E^{3.225}} \quad (4)$$

where P is the nominal contact pressure; L_1, the sliding distance; γ, the surface energy; E, the Young's modulus of elasticity for the polymeric material; and k, a proportionality constant.

1.1.2. Material Transfer

In the sliding of polymers against metal and glass surfaces, the wear process seems to be dominated by the phenomenon of the transfer of softer polymeric material to the harder counterface material. For example, a massive transfer of PTFE to clean glass surfaces occurring in the sliding process has been reported by Makinson and Tabor (23). Pooley and Tabor (24) found that lumps of PTFE and high density polyethylene transferred to glass and polished metal surfaces. They estimated the lumps to be several hundred Å in thickness.

The transfer of material has also been observed using infrared spectroscopy in polymer-polymer sliding. Sviridyonok et al. (25) observed that the transfer took place only under severe sliding conditions. They indicated that the direction of material transfer was governed by the peculiarities of molecular structure of the sliding pair. In a recent study, Jain and Bahadur (26) found that material transfer occurred under all sliding conditions. They concluded that the transfer of material was from a polymer of low-cohesive energy density to one of higher-cohesive energy density, and that the thickness of the transferred layer increased with increasing sliding speed and time but decreased with increasing normal load.

Bowers et al. (27) observed the transfer of a thin PTFE film to the steel surface, and established by electron diffraction the orientation of the film in the direction of sliding. Steijn (28) demonstrated by transmission electron microscopy the shearing of a thin film of PTFE in the sliding of a hardened steel indentor against a PTFE surface. These films were also found to have been oriented in the direction of sliding. Brainard and Buckley (29) used A.e.s.[2] to detect the transfer of a uniform and continuous film of PTFE, a few atomic layers thick, to a metal surface. Tanaka et al. (30) explained that the PTFE film is produced because of the slippage between crystalline slices of the banded structure of PTFE.

Working with polymers other than PTFE, Steijn (28) could not establish by transmission electron microscopy the typical shearing phenomenon which creates a thin film, as was observed in the case of a steel indentor sliding against a PTFE surface. Briscoe et al. (31) reported the presence of some film on a high density polyethylene surface when it was rubbed against a steel disc. The film here was not identified. Tanaka and Uchiyama (32) observed a thin polymer film in the sliding of low density polyethylene against a steel disc. They were able to establish by electron diffraction that the film was of low density polyethylene. Recently, Tanaka and Miyata (33) observed thin films of PTFE and a few other crystalline polymers when sliding was performed between abraded surfaces of these polymers and a clean glass plate. There was no attempt made to identify these films by electron diffraction.

---

[2] Auger emission spectroscopy.

1.1.3. Loose Wear Fragments

Apart from the transfer of material, loose wear fragments are also produced in the wear process. There is very little work reported in the literature on the study of these fragments. Most of the studies are confined to the qualitative observation of wear particles (34-38). As for the quantitative studies, Takagi and Tsuya (39) correlated the length of wear fragments with the rate of abrasive wear. Perhaps the best quantitative work on wear particles produced in an adhesive wear situation was done by Rabinowicz (40). His model considered a hemispherical wear particle, and assumed that an adhesive wear particle could be formed only when the total elastic energy contained in the particle under compressive loading was equal to or greater than the surface energy of the particle. On this basis, he derived the following equation for the diameter of wear particle:

$$d = \frac{24\gamma E}{\sigma_y^2} \tag{5}$$

where γ is the surface energy; E, the Young's modulus of elasticity; and σ_y, the yield strength of the particle material.

Soda et al. (41) observed that the shape of wear fragments formed in sliding between smooth metallic pairs was closer to a flattened ellipsoid than to a hemisphere. Rabinowicz (40) had also made similar observations, but considered hemispherical shape of the wear particle merely because of the simplicity. He has recently reported that the spherically-shaped wear particles result under uniaxial slow sliding conditions, as in fretting (42). The spherical shape is created here by the entrapment of particles inside the cavities of mating surfaces and by subsequent smoothening

from burnishing action.

Using the initial volume distribution of wear particles, and the statistical method for obtaining the relationship between the mean of the dimensions of the largest particles and that of the population as developed by Kimura (43), Soda et al. (41) calculated the number of wear fragments produced in a sliding process per unit time. From experimental and analytical studies of wear fragments and their relation to wear in general, they concluded that the variation in wear with normal load or sliding speed was due to the change in volume of the fragments and not in the number produced.

All of the studies on wear fragments reported above were done on metal pairs except the one by Rabinowicz (40). He measured the diameter of wear particles of PTFE and certain metallic materials sliding against the same materials in order to study the effect of surface energy and hardness on the wear particle size. In their study of abrasive wear of high density polyethylene sliding against steel, Bahadur and Stiglich (44) found that the wear rate increased with the size of wear particles.

1.1.4. Temperature Rise in Sliding and Its Effect on Wear

The temperature rise at the sliding surface is considered to affect the wear of polymeric materials much more significantly than that of the metallic materials because of their considerably lower thermal conductivity and melting points. Lancaster (12) attributed an abrupt increase in wear rate prior to failure to thermal softening of the thermoplastic substrate in the contact zone. Vinogradov et al. (45) observed thermosetting polymers becoming charred because of similar heating effects. Lancaster (12) found that the heat generated at the sliding interface depends more on speed than on load. Realizing this, several authors

(46-48) have studied the interface temperature rise phenomenon and its effect on wear at high sliding speeds.

The temperature rise problem in a sliding situation has been studied both analytically and experimentally. The first significant contribution came from Jaeger (49), who obtained temperature rise solutions for the case of sliding between two semi-infinite planes of different geometrical configurations. These equations have proved very useful in the prediction of temperature rise in situations such as metal cutting, where high normal stresses accompanied by plastic deformation are involved. Bowden and Tabor (50) developed similar equations for the calculation of temperature rise for a pin sliding on a finite plane. The application of both Jaeger's and Bowden and Tabor's solutions to the typical lightly-loaded sliding condition does not provide satisfactory agreement between the measured and calculated values of temperature rise (51).

Cook and Bhusan (51) developed an equation for the temperature rise between a pair of mating asperities, while ignoring the presence of other asperities in the sliding contact zone. They considered the interactive influence of temperature rise at other asperity locations on the contact situation. By combining the temperature contribution of interactive effects with the temperature rise at a single mating asperity pair, an equation for the resulting average temperature at an asperity contact was derived. Cook and Bhusan (51) reported a fair agreement between the predicted and the measured values of temperature rise for sliding situations where a metallic annulus rotated against a slotted annulus of a different metallic material. The analysis is not very useful from a practical standpoint because it involves the coefficient of friction, thermal properties,

hardness, and surface topography. The surface topography is difficult to estimate and is variable in sliding, and the hardness is meaningless for polymeric materials.

Archard (52) developed two different sets of equations for temperature rise at low speed and at high speed. Each of these sets consists of two equations, one for the elastic deformation and another for the plastic deformation in the contact zone. The applicability of these equations to a specific situation is determined by the magnitude of the dimensionless parameter "L" and the nature of deformation at the contact surface. This parameter L, originally introduced by Jaeger (49), is given by:

$$L = \frac{Va}{2\alpha}$$

where V is the sliding speed; a, the radius of circular contact area; and α, the thermal diffusivity of the moving surface. It was shown by Archard (52) to provide an indication of the depth of penetration of heat below the sliding interface. Archard (52) measured the flash temperature rise for sliding between pins and rings where both were made of 0.52% carbon steel. He found that the calculated values of flash temperature rise did not compare well with the measured ones. However, he succeeded in showing that when a perspex pin slid against a perspex ring, the onset of catastrophic wear rate corresponded to the temperature rise, as predicted by his equations, and that it was close to the thermal softening point of perspex. Later, Furey (53) measured the temperature rise between the surfaces of an AISI 52100 steel rotating cylinder (21 R_c, 0.2 μm CLA) and a stationary constantan ball (86 R_b, 0.15 μm CLA), and compared the experimental values with those calculated using

Archard's equations. He found that the predicted temperature rise values were 1.5 to 9 times the corresponding experimental values. This was true regardless of the contact area values used in Archard's equations which were estimated using the elastic or the plastic deformation in the contact zone.

Ling (54) used a probabilistic approach in conjunction with the principle of heat conduction to estimate the transient temperature at the sliding interface. For his model, he considered a semi-infinite solid with a square-shaped protrusion sliding against another body of an arbitrary shape, and asserted that the success of his model would not be affected by the shape of the slider. He assumed that the total real contact area for a specific load did not change with time, while the number of contacts and their locations did. The distribution of these contacts in space, as well as the variation of their positions with time, were both considered to be statistically random. The theoretical analysis has been supported with the experimental results for sliding between a rotating steel disc and a stationary acrylic cylinder.

The problem of temperature rise for the steady state condition at the sliding interface of a stationary pin and an infinitely long rotating cylinder was investigated theoretically by Kounas et al. (55). Assuming equality in average temperature at the pin and cylinder rubbing surfaces, they calculated the coefficient of distribution of frictional heat between these two bodies. The calculated coefficient was compared with the experimental values reported in the literature for a very few cases by these authors.

Harpavat (56) derived a steady state temperature rise equation for

the sliding interface between a plane of finite thickness and sliders of rectangular and trapezoidal shapes. He compared his results with the experimental data obtained for the case of an elastomeric trapezoidal slider rubbing against an aluminum substrate coated with chalcogenide material. The agreement was again off by a factor of 1.5 to 4.

El-Sherbiny and Newcomb (57) recently derived an equation for steady-state temperature rise at the interface between a rotating and a stationary cylinder, placed at right angles to each other. No experimental verification of this equation has been provided.

From the above, it can be seen that agreement between the measured and the predicted values of temperature rise at the sliding interface is generally lacking. The reason can be found in consideration of simplistic models to facilitate analytical solutions. For example, Jaeger's (49) formula, derived for semi-infinite solids, cannot be applied to situations where finite bodies are involved. Therefore, it is necessary to find separate solutions for different configurations and sliding situations, in order to realistically estimate the temperature rise in these cases.

1.2. Objective and Approach to the Problem

In a polymer-metal sliding system, interactions between polymer molecules and metal atoms at the sliding interface are responsible for the adhesive wear. This is further complicated by the dissipation of

frictional energy at the sliding interface. It may increase the molecular mobility, produce thermal softening or even cause degradation of the polymeric material in extreme cases. It appears that the temperature rise at the sliding interface is central to an understanding of the wear mechanism for polymer-metal combinations, because polymers are more susceptible to change even with mild increases in temperature.

A major part in this research concentrated on the realistic estimate of temperature rise at the sliding interface under varying speed and load conditions. A steady state heat transfer model was developed for the experimental configuration of a pin and a disc. The model considers the conduction of heat from the sliding contact zone in both the pin and the radial direction of the disc, together with the heat loss by convection from the sides and the periphery of the disc. It was followed by the measurement of temperature rise at the rubbing surface for both the steady and unsteady state conditions. The measurements also helped in the verification of the analytical solutions obtained for the model. Since both the analytical and experimental approaches provide only the average temperature rise, further investigation of the probable thermal softening or degradation at the asperity contacts was carried out using DTA technique.

The nature of deformation in the contact region was investigated using electron microscopy techniques. Thus, for low-speed conditions, transmission electron microscopy was used to study the nature of deformation and the formation of films in the sliding process. The deformation occurring under high-speed conditions was more severe and was studied

at lower magnifications by scanning electron microscopy. The nature and size of the films and the wear particles formed were also studied. From the measurements of particle size, the thickness of wear particles was estimated using an equation derived for the purpose.

Finally, based upon the above investigations, the wear mechanisms for different speed conditions were proposed. The wear model is based on the understanding of the morphological structure of polymeric materials.

2. ANALYTICAL METHODS

2.1. Formulation of the Heat Transfer Model

The sliding system used in the experimental investigation consists of a thin rotating steel disc sliding against a stationary cylindrical polymer pin. Here heat is generated at the interface as a result of frictional resistance. It is desirable to develop an equation for temperature rise at the sliding interface of this system.

Figure 2(a) shows a thin disc of radius R in stationary condition and in contact with a cylindrical pin of diameter d with coordinates (r,θ) fixed to the disc. The same disc rotating about its center and sliding on its periphery against the flat end of the stationary pin is shown in Figure 2(b) with coordinates (r,ψ) in reference to the pin. The angle of contact between the pin and the disc is represented by Ω. Assumptions:

1. The periodic heating at the disc periphery has caused a steady oscillation in temperature in the thin annular part of the disc.
2. The temperature of the disc varies along its radius and circumference. Since the width of the disc is considered to be small, the heat flow by conduction in the axial direction is neglected.
3. The heat loss by convection occurs from the exposed periphery of the disc not in direct contact with the pin surface. There is also heat loss from the sides.
4. The amount of heat carried away by the polymer wear particles is negligibly small.
5. Since the diameter of the pin is small, the temperature is assumed to be uniform in any cross section.

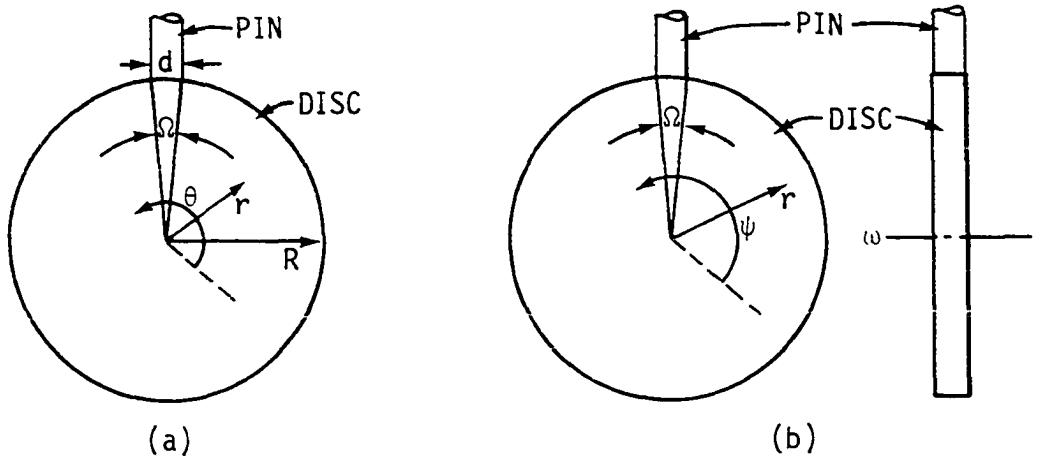

Fig. 2. Schematic representation of pin-and-disc sliding system; (a) both disc and pin stationary with coordinates (r,θ) fixed to the disc, (b) rotating disc and stationary pin with coordinates (r,ψ) in reference to the pin.

6. A part of the cylindrical surface, as well as the flat end of the pin, are in contact with the aluminum holder. The contacting portions of the pin are assumed to be at room temperature.
7. The average temperature of the pin rubbing surface is equal to that of the disc rubbing surface in the contact zone.
8. The entire surface of the end of the pin is in contact with the disc.
9. There is no phase change occurring in the pin material at the rubbing surface.

2.2. Heat Transfer Equation for the Rotating Disc

The steady state heat transfer equation in cylindrical coordinates for the disc in the system described (Figure 2(a)) is

$$\frac{\partial^2 T}{\partial r^2} + \frac{1}{r}\frac{\partial T}{\partial r} + \frac{1}{r^2}\frac{\partial^2 T}{\partial \theta^2} = 0 \qquad (6)$$

where T is the temperature rise at any location, and (r,θ) is the coordinate system fixed in the disc. In order to take into consideration the effect of rotation of the disc, which has an angular velocity of ω rad/sec, the coordinate system is changed to (r,ψ), where the latter is considered fixed with respect to the heat source. Thus, in the new coordinate system the above equation becomes

$$\frac{\partial^2 T}{\partial r^2} + \frac{1}{r}\frac{\partial T}{\partial r} + \frac{1}{r^2}\frac{\partial^2 T}{\partial \psi^2} = 0 \qquad (7)$$

where the two systems of coordinates are related to each other by

$$\psi = \theta - \omega T$$

with T as the time under consideration.

In order to consider the heat loss by convection from the sides of the disc, Equation (7) is modified as follows:

$$\frac{\partial^2 T}{\partial r^2} + \frac{1}{r}\frac{\partial T}{\partial r} + \frac{1}{r^2}\frac{\partial^2 T}{\partial \psi^2} - \frac{2h'T}{K_d t} = 0 \qquad (8)$$

where h' is the film heat transfer coefficient for the sides of the disc; K_d, the thermal conductivity of the disc material; and t, the thickness of the disc. Substituting σ^2 for $\frac{2h'}{K_d t}$ in the above equation, we get

$$\frac{\partial^2 T}{\partial r^2} + \frac{1}{r}\frac{\partial T}{\partial r} + \frac{1}{r^2}\frac{\partial^2 T}{\partial \psi^2} - \sigma^2 T = 0 \qquad (9)$$

A solution in the following form is chosen to solve Equation (9)

$$T = R(r)\ \phi\ (\psi) \qquad (10)$$

Differentiating the above equation and substituting the result in Equation (9), we get

$$\phi \frac{d^2 R}{dr^2} + \frac{1}{r}\phi \frac{dR}{dr} + \frac{1}{r^2} R \frac{d^2 \phi}{d\psi^2} = \sigma^2 R\phi$$

or $$r^2 \frac{R''}{R} + r \frac{R'}{R} - r^2\sigma^2 = -\frac{\phi''}{\phi} \qquad (11)$$

where $$R'' = \frac{d^2 R}{dr^2}\ ;\quad R' = \frac{dR}{dr}\ ;\quad \phi'' = \frac{d^2\phi}{d\psi^2}\ .$$

Since the left-hand side of Equation (11) does not have ψ and the right-hand side does not have r, and since they are equal, each side may be equated to a constant, say λ^2. Then

$$r^2 \frac{R''}{R} + r \frac{R'}{R} - r^2\sigma^2 - \lambda^2 = 0 \tag{12}$$

and $$\varphi'' + \varphi\lambda^2 = 0 \tag{13}$$

The solution of Equation (12) is of the form

$$R = AI_\lambda (\sigma r) + BK_\lambda (\sigma r) \tag{14}$$

where I_λ and K_λ are modified Bessel functions of the first and second kind of order λ.

The general solution for Equation (13) is:

$$\varphi = C \cos \lambda\psi + D \sin \lambda\psi \tag{15}$$

where A, B, C and D are constants.

Combining Equations (14) and (15), the solution for Equation (9) may be written as:

$$T = [AI_\lambda(\sigma r) + BK_\lambda(\sigma r)][C \cos \lambda\psi + D \sin \lambda\psi] \tag{16}$$

Putting $\lambda=n$ where $n \geq 0$, Equation (16) becomes

$$T = [AI_n(\sigma r) + BK_n(\sigma r)][C \cos n\psi + D \sin n\psi] \tag{17}$$

Writing $AC = a_n$, $AD = b_n$, $BC = c_n$, and $BD = d_n$, the above equation becomes

$$T = [a_n I_n(\sigma r) \cos n\psi + b_n I_n(\sigma r) \sin n\psi$$

$$+ c_n k_n(\sigma r) \cos n\psi + d_n k_n(\sigma r) \sin n\psi]$$

so that for n=0, we get

$$T = [a_0 I_0(\sigma r) + c_0 k_0(\sigma r)]$$

and for n = 1,2,3...∞, we get

$$T = I_n(\sigma r)\ [a_n \cos n\psi + b_n \sin n\psi] + K_n(\sigma r)$$

$$[c_n \cos n\psi + d_n \sin n\psi]$$

as a set of particular solutions.

The temperature rise equation may thus be written as

$$T = [a_0 I_0(\sigma r) + C_0 K_0(\sigma r)] + \sum_{n=1}^{\infty} [I_n(\sigma r)$$

$$(a_n \cos n\psi + b_n \sin n\psi)$$

$$+ K_n(\sigma r)(c_n \cos n\psi + d_n \sin n\psi)] \qquad (18)$$

2.3. Boundary Conditions

1. Since the pin is stationary and the disc is rotating, heating at any point on the disc periphery is periodic in nature. The temperature field equation for periodic heating for a semi-infinite slab (58) is given by

$$t_1 = t_s\, e^{-\sqrt{\frac{\pi}{\alpha \tau_0}}\, x} \cdot \cos\left(\sqrt{\frac{\pi}{\alpha \tau_0}}\, x - 2\pi \frac{\tau}{\tau_0}\right) \qquad (19)$$

where t_s is the amplitude of surface temperature; α, the thermal diffusivity; τ_0, the period of temperature oscillation; τ, the time; and x, the depth of the slab.

It can be seen from the above equation that the advancing temperature wave decreases in amplitude with increasing depth by a factor $\exp\left(-\sqrt{\frac{\pi}{\alpha\tau_0}}\, x\right)$.

The wavelength of the above cosine wave is given by

$$\lambda_1 = 2\sqrt{\pi\alpha\tau_0} \tag{20}$$

From the plots of x/λ_1 as abscissa and t_1/t_s as ordinate, it is found (58) that the depth x, where the amplitude is reduced to a very small fraction of that on the surface, is given by

$$x = 1.6\sqrt{\pi\alpha\tau_0} \tag{21}$$

Taking $\alpha = 0.085$ cm^2/sec for the disc material and $\tau_0 = 0.3$ sec, which is the time of rotation for a disc rotating at 200 rpm (speeds used in the experimental investigation ranged from 50 to 500 rpm), x was calculated as 4.5 mm. Since this depth is very small compared to the radius of the disc, the portion of the disc affected by the temperature oscillation has a small curvature. As such, the application of the above equations, to the arrangement being considered will not produce any appreciable error. Since the temperature rise affects a very small depth below the disc periphery, the disc may be considered as having two parts, one an annulus of inside radius R_1 and outside radius R, and the other a cylindrical disc of radius R_1. It may further be assumed that the temperature gradient in the radial direction in the latter portion of the disc is zero. This leads to the following boundary condition:

At $r = R_1$, $\frac{\partial T}{\partial r} = 0$, so that from Equation (18)

$$\left.\frac{\partial T}{\partial r}\right|_{r=R_1} = \left[a_0 \frac{dI_0(\sigma r)}{dr} + c_0 \frac{dK_0(\sigma r)}{dr}\right]_{r=R_1}$$

$$+ \sum_{n=1}^{\infty} \left[\frac{dI_n(\sigma r)}{dr}(a_n \cos n\psi + b_n \sin n\psi)\right.$$

$$\left. + \frac{dK_n(\sigma r)}{dr}(c_n \cos n\psi + d_n \sin n\psi)\right]_{r=R_1} \qquad (22)$$

Putting

$$\left.\frac{dI_0(\sigma r)}{dr}\right|_{r=R_1} = p_0$$

$$\left.\frac{dK_0(\sigma r)}{dr}\right|_{r=R_1} = q_0$$

$$\left.\frac{dI_n(\sigma r)}{dr}\right|_{r=R_1} = p_n$$

$$\left.\frac{dK_n(\sigma r)}{dr}\right|_{r=R_1} = q_n$$

the following relationships are obtained from Equation (22)

$$a_0 p_0 + c_0 q_0 = 0 \qquad (23)$$

$$a_n p_n + c_n q_n = 0 \qquad (24)$$

$$b_n p_n + d_n q_n = 0 \qquad (25)$$

Writing from the above equations

$$\frac{a_0}{q_0} = -\frac{c_0}{p_0} = -1_0$$

$$\frac{a_n}{q_n} = -\frac{c_n}{p_n} = -1_n$$

$$\frac{b_n}{q_n} = -\frac{d_n}{p_n} = -m_n$$

and substituting in Equation (18), we get

$$T = 1_o\,[p_0K_0(\sigma r)-q_0I_0(\sigma r)] + \sum_{n=1}^{\infty} [1_n\{p_nK_n(\sigma r) - q_nI_n(\sigma r)\}\cos n\psi + m_n\{p_nK_n(\sigma r) - q_nI_n(\sigma r)\}\sin n\psi] \quad (26)$$

2. The secondary boundary condition is obtained from the consideration that a part of the heat generated at the sliding interface is lost through the periphery of the disc by convection and the remainder is conducted radially inwards. Thus we get

$$A'K_d \frac{\partial T}{\partial r} = A_0\gamma_1 q'(\psi) - A'hT \quad (27)$$

at r = R, where $A'-A_0 \simeq A'$, because A_0 is negligibly small compared to A'.

Here

A' = peripheral area, $2\pi Rt$

A_0 = area over which heat is generated, i.e., the area of the pin-disc contact surface

h = film heat transfer coefficient for periphery of the disc

$q'(\psi)$ = heat flux (heat generated per second per unit area)

and γ_1 = heat distribution coefficient, i.e., the fraction of heat generated going into the disc.

Dividing Equation (27) by $A'K_d$, we get

$$\frac{\partial T}{\partial r} = \frac{A_0 \gamma_1 q'(\psi)}{A'K_d} - \frac{h}{K_d} T$$

Substituting $\frac{h}{K_d} = H$ and $A_0 q'(\psi) = q$, we get

$$\frac{\partial T}{\partial r} + HT = \frac{\gamma_1 q}{A'K_d} = F \tag{28}$$

where q is the heat generated per second due to friction and is given by

$$q = \frac{\mu NV}{J}$$

where μ is the coefficient of friction; N, the normal load; V, the sliding speed; and J, the mechanical equivalent of heat.

The right hand side of Equation (28) can be expanded into a Fourier series of period 2π as

$$F = F_0 + \sum_{n=1}^{\infty} (F_n \cos n\psi + G_n \sin n\psi) \tag{29}$$

Differentiating Equation (26) with respect to r and substituting the result in Equation (28), we get

$$\begin{aligned} & l_0 \left[\left(\frac{\partial}{\partial r} + H \right) \{ p_0 K_0(\sigma r) - q_0 I_0(\sigma r) \} \right]_{r=R} \\ & + \sum_{n=1}^{\infty} l_n \left[\left(\frac{\partial}{\partial r} + H \right) \{ p_n K_n(\sigma r) - q_n I_n(\sigma r) \} \right]_{r=R} \cos n\psi \\ & + \sum_{n=1}^{\infty} m_n \left[\left(\frac{\partial}{\partial r} + H \right) \{ p_n K_n(\sigma r) - q_n I_n(\sigma r) \} \right]_{r=R} \sin n\psi \\ & = F_0 + \sum_{n=1}^{\infty} (F_n \cos n\psi + G_n \sin n\psi) \end{aligned} \tag{30}$$

Equating the coefficients on both sides of the above equation, we get

$$F_0 = l_0\left[p_0\left\{\frac{dK_0(\sigma r)}{dr} + HK_0(\sigma r)\right\}\right.$$

$$\left. - q_0\left\{\frac{dI_0(\sigma r)}{dr} + HI_0(\sigma r)\right\}\right]_{r=R}$$

or

$$l_0 = \frac{F_0}{[p_0\{-\sigma K_1(\sigma R) + HK_0(\sigma R)\} - q_0\{\sigma I_1(\sigma R) + HI_0(\sigma R)\}]} \qquad (31)$$

Similarly,

$$F_n = l_n\left[\left(\frac{\partial}{\partial r} + H\right)\{p_n K_n(\sigma r) - q_n I_n(\sigma r)\}\right]_{r=R}$$

or

$$l_n = \frac{F_n}{[p_n\{-\sigma K_{n-1}(\sigma R) - \frac{n}{R}K_n(\sigma R) + HK_n(\sigma R)\} - q_n\{\sigma I_{n-1}(\sigma R) - \frac{n}{R}I_n(\sigma R) + HI_n(\sigma R)\}]} \qquad (32)$$

and

$$G_n = m_n\left[\left(\frac{\partial}{\partial r} + H\right)\{p_n K_n(\sigma r) - q_n I_n(\sigma R)\}\right]_{r=R}$$

or

$$m_n = \frac{G_n}{[p_n\{-\sigma K_{n-1}(\sigma R) - \frac{n}{R}K_n(\sigma R) + HK_n(\sigma R)\}}$$

$$- q_n\{\sigma I_{n-1}(\sigma R) - \frac{n}{R}I_n(\sigma R) + HI_n(\sigma R)\}] \qquad (33)$$

Denoting the denominators of Equation (31) as x_o and those of equations (32) and (33) as x_n, we may write

$$l_0 = \frac{F_0}{x_0}$$

$$l_n = \frac{F_n}{x_n} \tag{34}$$

and

$$m_n = \frac{G_n}{x_n}$$

Substituting the values of l_0, l_n and m_n from the above into Equation (26), the temperature rise at the rubbing surface of the disc is given by

$$T\Big|_{r=R} = \frac{F_0}{x_0}[p_0 K_0(\sigma R) - q_0 I_0(\sigma R)] + \sum_{n=1}^{\infty} [\frac{F_n}{x_n}\{p_n K_n(\sigma R) - q_n I_n(\sigma R)\} \cos n\psi + \frac{G_n}{x_n}\{p_n K_n(\sigma R) - q_n I_n(\sigma R)\} \sin n\psi] \tag{35}$$

Since the heat on the disc surface is generated only when it is in contact with the pin, we may write

$$\gamma_1 q = Q_1 \quad \text{for } 0<\psi<\Omega$$

$$= 0 \quad \text{for } \Omega<\psi<2\pi$$

The value of Ω can be calculated from

$$\Omega \simeq \frac{d}{R}$$

where d is the diameter of the pin.

The values of the coefficients, F_0, F_n and G_n in Equation (29) are to be evaluated as follows:

$$F_0 = \frac{1}{2\pi}\int_0^{2\pi} F d\psi$$

$$= \frac{1}{2\pi}\int_0^{\Omega} \frac{Q_1}{A'K_d}\, d\psi + \frac{1}{2\pi}\int_{\Omega}^{2\pi} 0 d\psi$$

$$= \frac{\Omega\gamma_1 q}{2\pi A'K_d} \tag{36}$$

$$F_n = \frac{1}{\pi}\int_0^{2\pi} F \cos n\psi d\psi$$

$$= \frac{1}{\pi}\int_0^{\Omega} \frac{Q_1}{A'K_d} \cos n\psi d\psi$$

$$= \frac{B_n\gamma_1 q}{\pi A'K_d} \tag{37}$$

Similarly,

$$G_n = \frac{1}{\pi}\int_0^{2\pi} F \sin n\psi d\psi$$

$$= \frac{\gamma_1 q}{\pi A'K_d}\left[-\frac{1}{n}\cos n\psi\right]_0^{\Omega}$$

$$= \frac{B'_n\gamma_1 q}{\pi A'K_d} \tag{38}$$

2.4. Heat Distribution Coefficient

In order to calculate the temperature rise using Equation (35), the heat distribution coefficient is needed. This is the ratio of the amount of heat energy flowing into the disc to the total heat generated at the sliding interface. If $\gamma_1 q$ is the amount of heat energy flowing into the

disc, then $(1-\gamma_1)q$ will be the amount of heat flowing into the pin where the heat carried out by wear particles is assumed to be negligible.

Considering the heat transfer by conduction along the length of the pin and by convection from the periphery, the differential equation (58) for temperature distribution in a pin of length l, cross-sectional area A_0, and perimeter p is given by

$$\frac{\partial^2 t}{\partial x^2} - \frac{h_1 p}{K_p A_o}(t-t_f) = 0 \tag{39}$$

where K_p = thermal conductivity of the pin material

t = temperature in the pin at any axial distance x

t_f = ambient temperature

h_1 = heat transfer coefficient for the pin.

Substituting

$$T = t-t_f$$

and

$$m = \sqrt{\frac{h_1 p}{K_p A_o}}$$

in the above equation, we get

$$\frac{\partial^2 t}{\partial x^2} - m^2 T = 0 \tag{40}$$

The general solution of this equation is

$$T = Ae^{mx} + Be^{-mx} \tag{41}$$

The boundary conditions are as follows:

(1) at $x = 0$ (i.e. at the interface), $T = T_p$

(2) at $x = \ell$, $T = 0$ (i.e. no temperature rise)

With these two conditions, the temperature distribution equation becomes

$$T(x) = \frac{T_p \sinh m(\ell - x)}{\sinh (m\ell)} \tag{42}$$

where T_p is the temperature of the pin rubbing surface.

Now the rate of heat flow into the pin at $x = 0$ is given by

$$Q_2 = -A_0 K_p \left.\frac{dT}{dx}\right|_{x=0}$$

$$= \frac{A_0 T_p K_p m}{\tanh (m\ell)} \tag{43}$$

Putting $N_1 = ml$ in the above equation, we get

$$T_p = \frac{Q_1 \ell \tanh (N_1)}{A_0 K_p N_1} \tag{44}$$

Substituting $Q_2 = (1-\gamma_1)q = \frac{(1-\gamma_1)\mu NV}{J}$ from Equation (29), we get

$$T_p = \frac{(1-\gamma_1)\,\mu NV\,\ell \tanh (N_1)}{A_0 K_p N_1} \tag{45}$$

Putting the value of q from Equation (29) and the values of F_o, F_n and G_n from Equations (36, 37 and 38), respectively, in Equation (35), the temperature rise in the disc rubbing surface is given by

$$T\Big|_{r=R} = T_D = \frac{\mu NV\gamma_1}{\pi JA' K_d} \cdot S \tag{46}$$

where

$$S = [\frac{\Omega}{2x_0}\{p_0K_0(\sigma R) - q_0I_0(\sigma R)\} + \sum_{n=1}^{\infty}\frac{B_n}{x_n}\{p_nK_n(\sigma R) - q_nI_n(\sigma R)\}\cos n\psi + \sum_{n=1}^{\infty}\frac{B'_n}{x_n}\{p_nK_n(\sigma R) - q_nI_n(\sigma R)\}\sin n\psi]$$

Considering the equality of temperature at both the pin and disc rubbing surfaces,

i.e., $T_p = T_D$

we get

$$\gamma_1 = \frac{\pi A' K_d \ell \tanh (N_1)}{K_p A_o N_1 S + \pi A' K_d \ell \tanh (N_1)} \qquad (47)$$

The above equation demonstrates that the heat distribution coefficient depends upon the dimensions, thermal conductivities and heat transfer coefficients of the sliding members.

2.5. Heat Transfer Coefficients

The heat transfer coefficient h for the disc periphery is required for the calculation of x_o and x_n in Equation (46), whereas the coefficient h' for the sides of the disc is needed to compute the argument σ in the same equation.

Due to the lack of data on transfer of heat from the periphery of a rotating disc, the heat transfer coefficient h was estimated from several studies (59-61) on the heat transfer from rotating cylinders. These studies report that, at rotational Reynolds numbers (based on

diameter) of less than 1,000, the heat transfer is virtually unaffected by rotation but is totally controlled by free convection or the Grashof number. In the Reynolds number range 1,000-10,000, both the rotational Reynolds number and the Grashof number govern heat transfer, though the effect of the Grashof number starts to decrease beyond a Reynolds number or about 1,000. For Reynolds numbers higher than 10,000, it is the Reynolds number alone that is important. Thus, in estimating the value of h up to a Reynolds number of 10,000, the following correlation for calculation of the Nusselt number, as proposed by Etemad (60), may be used:

$$Nu = 0.11[(0.5\ Re^2 + Gr)\ .\ Pr]^{0.35} \tag{48}$$

where

Re = rotational Reynolds number, $\frac{VD_d}{\nu}$

Nu = Nusselt number, $\frac{hD_d}{k_a}$

Gr = Grashof number, $\frac{\beta g \Delta t\ D_d^3}{\nu^2}$

Pr = Prandtl number, $\frac{C_p \mu_v}{K_a}$

Where V is the speed; D_d, the diameter of disc; Δt, the temperature difference; and g, the acceleration due to gravity. Here ν, k_a, β, C_p and μ_v denote the kinematic viscosity, thermal conductivity, coefficient of thermal expansion, specific heat and dynamic viscosity of air, respectively, all of which are evaluated at the film temperature. Since a prior knowledge of the temperature rise is needed to calculate the Grashof number, it is desirable to estimate the Nusselt number without taking the

Grashof number under consideration. A justification for this is provided in Section 4. Since the Grashof number is negligible for Reynolds numbers higher than 10,000, the same equation ignoring the Grashof number will be used in these calculations.

The heat transfer coefficient h' for the sides of the disc can be calculated using the following correlation by Richardson and Saunders (62):

$$Nu = \frac{h'R}{K_a} = 0.40\ (Re^2 + Gr)^{1/4} \qquad (49)$$

where the Reynolds and the Grashof numbers are for the disc radius.

The heat transfer equation developed here has been verified experimentally in Section 4.

3. EXPERIMENTAL PROCEDURE

3.1. Sliding Experiments

3.1.1. Experimental Set-Up

The sliding experiments at high speeds (0.5 m/sec and above) were performed in a pin-and-disc type machine, shown in Figure 3(a). It consists of a disc (9.85 cm dia and 6.8 mm thick) of AISI 4340 steel, hardened and ground (R_c 55 and 0.2 μm RMS), which is keyed to a motor shaft. The speed of the motor can be varied from about 50 rpm to 2500 rpm by a speed controller. A polymer pin (2.0 cm long, 6.3 mm dia) rides on the rotating disc and provides a sliding motion between the two. The load on this pin is applied by dead weights supported at the end of a horizontal beam. A leverage of 4:1 is achieved at the polymer specimen, which is secured to the vertical member with a holder. The vertical member carries two strain gages which allow for the measurement of friction force arising from the sliding motion between the steel disc and the polymer specimen. The output of the strain gages is amplified, and recorded by a Brush Mark 220 recorder.

A tribometer (63), was used to perform sliding at a very low speed of 0.002 m/sec, to avoid heating at the interface. Such a low sliding speed could not be obtained in the pin-and-disc type machine. The sliding in the tribometer was performed between a polymer disc and a hemispherical steel indentor. The polymer disc is screwed to a brass disc which derives rotary motion from a reversible speed 1/3 hp motor through a reduction gear box. The indentor is attached to a cantilever arm which is hinged to a saddle that traverses on two fixed guides when a screw rod is turned. This provides an arrangement for changing position of the

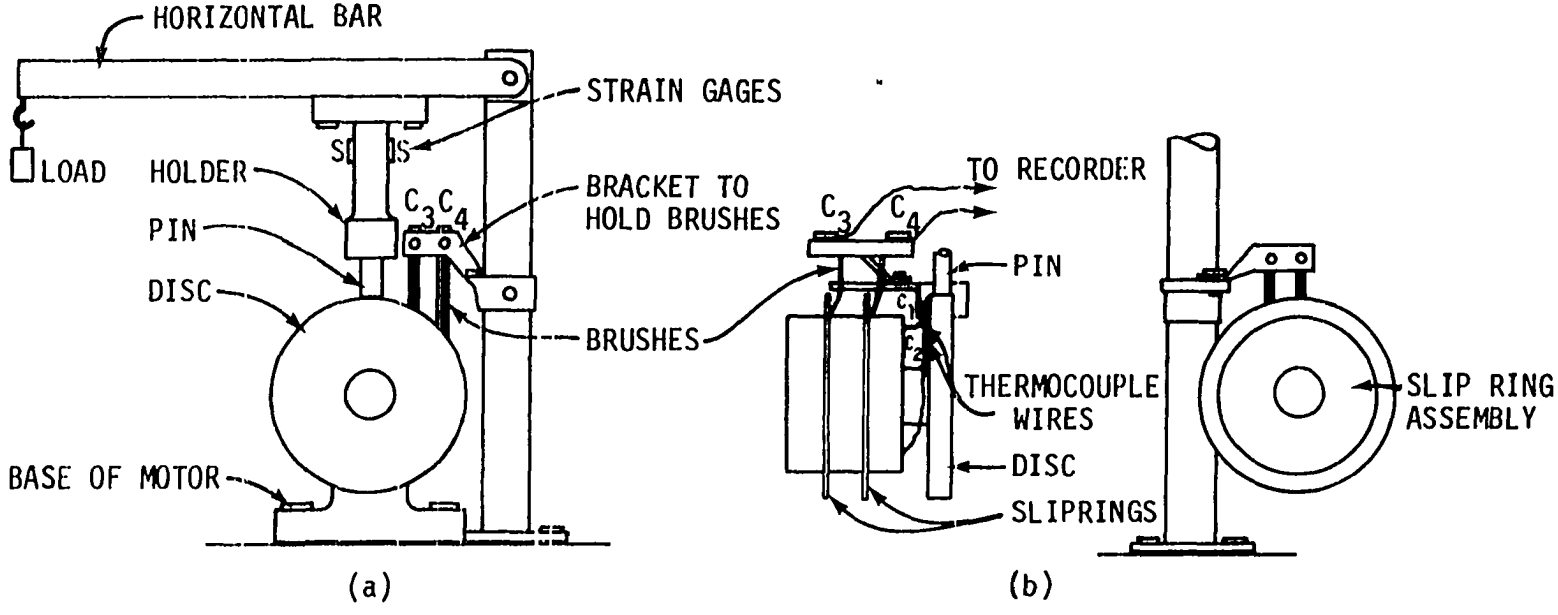

Fig. 3. Schematic of pin-and-disc machine showing (a) the sliding system; (b) the details of slip ring and brush arrangement for temperature measurement.

indentor on the flat surface of the polymeric disc specimen. The indentor is loaded through a lever mechanism by a combination of dead weights.

3.1.2. Temperature Measurements

The temperature measurements were performed for high speed conditions only in the pin-and-disc type machine (Figure 3(a)). The arrangement consisted of a thermocouple junction of very fine wires (3 mil dia), snug-fitted into a 0.6 mm diameter hole drilled from the side at about 1.5 mm distance from the sliding end of the polymer pin. The leads were connected to an automatic Speedomax W/L Leeds and Northrup temperature recorder.

In order to determine that the thermocouple junction was in good contact with the surrounding pin material, and that the measured temperature was not erroneous, a polymer slab was compression molded with thermocouple junctions in it. The cylindrical specimens, with a thermocouple junction in each, were machined and later used for the measurement of temperature. The temperature rise values were found to be in close agreement for both arrangements.

The problem with both arrangements was that the rapid wear of the polymer pin exposed the thermocouple junction to the disc surface at times. Furthermore, the distance between the junction and the rubbing surface was changing continuously. It was, therefore, decided to use the slip ring and brush assembly shown in Figure 3(b). It consists of a thermocouple junction A (Figure 4), embedded in the rotating disc at a depth of about 15 mil from the sliding surface. The slant hole in the disc was drilled at about 30 mil from the peripheral surface at an angle

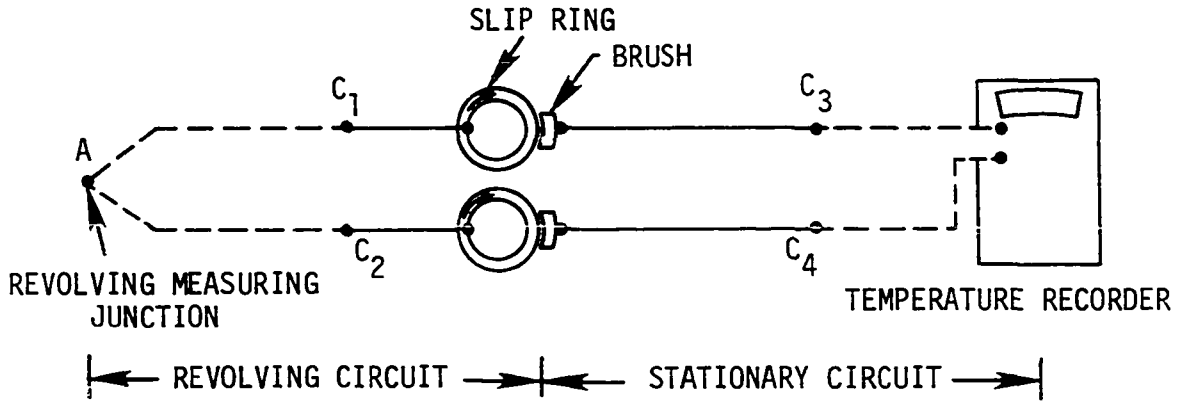

Fig. 4. Schematic diagram of temperature measuring system.

of approximately 80° with the radial direction of the disc. The thermocouple wires are connected to the slip rings through C_1 and C_2. This whole arrangement constitutes the revolving circuit. The stationary part of the circuit consists of brushes which are connected to the temperature recorder through C_3 and C_4.

The measuring system was calibrated by immersing the disc (with the thermocouple junction in it) in a stationary condition in the reference temperature baths of ice water and boiling water. The generation of any stray emf in the system due to heating at the slip ring-brush contacts was checked by rotating the disc at different speeds. No temperature rise was noticed during the first few seconds. As an additional check, after a steady-state temperature condition had been obtained at the rubbing surface, the disc was stopped. Again, no change in temperature was noticed. It was thus concluded that no significant stray emf was being generated due to rotation of the disc. This agrees with the observation of Tarr (64), who found that the stray emf produced a negligible ± 0.8°C (maximum) difference for a speed of 27.5 m/sec.

Using this system, the temperature rise corresponding to both the steady and the unsteady state heat transfer conditions was measured for each combination of the sliding speeds, 0.25, 0.5, 1.0, 1.5, 2.5 and 4.0 m/sec, and the loads, 1150, 1650 and 2750 g. The coefficient of friction was also measured using the strain gage arrangement shown in Figure 3(a).

3.2. Material Selection

The polymeric materials selected for the present work were high density polyethylene, polyoxymethylene, PTFE, polypropylene and poly-

carbonate. The selection was guided by the consideration that all of these materials are extensively used in applications where sliding or a combination of sliding and rolling motions are involved. For example, crystalline polymers, namely, polyethylene, polyoxymethylene, polypropylene and PTFE, are commonly used for bearings, bushings, slides, guides, valve liners, gears, cams, etc. Since failure due to wear limits the usefulness of these parts, an understanding of the mechanism of wear failure was considered technologically important.

In addition to the above materials, polycarbonate (which is an amorphous polymer) was also included in some wear studies to provide an idea of the mechanisms of wear for both the crystalline and amorphous polymers.

3.3. Specimen Preparation for Sliding Experiments

The polymer pins were machined from about 35 mm diameter extruded rods bought from Cadillac Plastics and Chemical Co. The rubbing surface of the pin was finished by polishing with 240, 400 and 600 grade emery papers under running water. The surface was examined in an optical microscope to ensure that it was free from the embedded particles detached during polishing. After cleaning the surface with distilled water and isopropyl alcohol, the pins were stored in a desiccator for about 12-14 hours before testing. The steel disc was machined from a 12 cm dia rod of AISI 4340 steel. It was hardened to 55 R_c, and the periphery was finished smooth to about 0.2 μm RMS by grinding. The polymer discs were machined from about 12 mm thick sheets bought from Cadillac Plastics and Chemical Co. The surface of the disc was abraded with 600 grade emery

paper using radial strokes to produce abrasion grooves in the radial direction. The hemispherical metallic indentor was made from a low carbon steel. It was finished smooth by grinding and polishing operations and then cleaned with isopropyl alcohol.

3.4. Differential Thermal Analysis (DTA) Measurements

The material removed from the polymer pin sliding surfaces was analyzed by DTA in order to detect whether softening or melting takes place in the immediate layer of the rubbing surface of the polymer pin. Here a Rigaku differential thermal analyzer was used with powdered alumina as the reference material. The heating rate was set at 5°C/min, and the range was 100 μV. In order to produce samples for DTA, rubbing was performed in the pin-and-disc type machine under a constant load of 2750 g, and the sliding speed was varied from 1.5 to 4 m/sec. Thus, the sample for DTA consisted of fragmented polymeric material produced as a result of sliding. In cases where pins failed because of excessive deflection under severe sliding conditions, enough of the fragmented material was obtained. Under less severe conditions when such failure did not occur, some material had to be obtained by scraping the sliding tip of the pin. The weight of each sample used for differential thermal analysis was kept approximately the same. The analysis was repeated several times to ensure the correctness of the data.

3.5. Surface Examination

3.5.1. Scanning Electron Microscopy

The sliding surfaces of the polymer pins were examined in a scanning electron microscope in order to study the nature of deformation occurring at the rubbing surface. The samples were prepared by coating the sliding surfaces with C and Au under a vacuum to reduce charging. The accelerating voltage used in the electron microscopy work was between 5 and 10 kV to minimize radiation damage.

3.5.2. Transmission Electron Microscopy

Transmission electron microscopy of the sliding surface was carried out to study the nature of wear under low speed conditions. Here the sliding was performed between a polymer disc with radial abrasion marks and a steel indentor in the tribometer. When the disc rotated about its center, the sliding direction was at about a 90° angle to the abrasion marks. The sliding conditions chosen consisted of a load of 1600 g, a speed of 0.002m/sec, and a time of 20 min. Replicas for examination in the microscope were made from both the sliding track and out-of-the-track portions. A conventional replication technique was used. It involved shadowing the surface in a vacuum with Ge, sputtering with C, deposition of a thin layer of 3% aqueous solution of polyacrylic acid (PAA), and removal from the polymer surface of the dried layer, which was floated later on distilled water so that the PAA could be dissolved. The extraction replica thus consisted of shadowed Ge with a backing of carbon.

A sketch of a polymer disc showing the abrasion marks, wear tracks and replicated areas is shown in Figure 5.

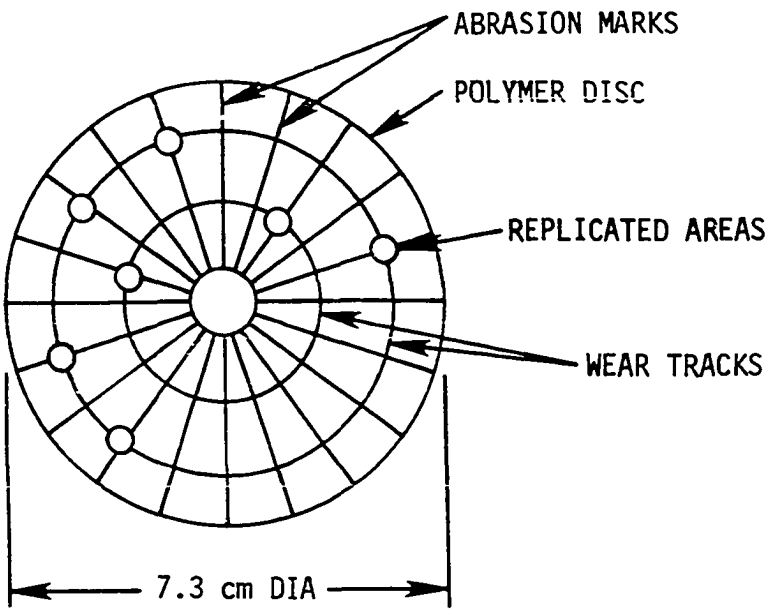

Fig. 5. Sketch of polymer disc showing the abrasion marks, wear tracks and replicated areas.

3.6. Measurement of Wear Particle Size

The loose polymer wear particles collected on the aluminum pin holder were used for measuring the size of wear particles. The measurements were carried out on all particles located in an arbitrarily selected area, using a Bausch and Lomb optical microscope. The particle dimensions were measured in two directions perpendicular to each other.

In the experiments performed on the pin-and-disc machine, the load was varied from 920 g to 1720 g in 200 g increments. The sliding speed was kept constant at 0.5 m/sec to minimize the heating effect. The sliding time was about an hour.

4. TEST RESULTS AND DISCUSSION

4.1. Temperature Rise at the Disc Rubbing Surface

4.1.1. Measured Temperature Rise

It has been noted that temperature at the rubbing surface was measured under varying load and sliding speed conditions, using a thermocouple with its junction located at about 0.3 mm below the surface. Since the disc material is highly conductive, the average temperature on the rubbing surface should be very close to the measured temperature. The temperature measurement was carried out in order to determine the extent temperature was controlling the wear mechanism. Since polymers have considerably lower softening or melting points than other materials, even moderate values of temperature rise at the rubbing surface are likely to produce softening and thus lead to a catastrophic wear failure.

The variation of temperature with time for different sliding speeds and load combinations is shown in Figures 6-9 for high density polyethylene, polyoxymethylene, PTFE and polypropylene, respectively. Here the sliding conditions were chosen with the objective of covering both the steady state and unsteady state conditions, so that the transition from steady state to unsteady state could be studied. It was not practical to get the unsteady state data for polypropylene because of excessive stick-slip motion. As for polycarbonate, the stick-slip motion occurred even at the lowest sliding speed (0.25 m/sec) used in this experimental investigation. For this reason, temperature measurements on this material were not carried out.

A transition from steady state to unsteady state was observed in the

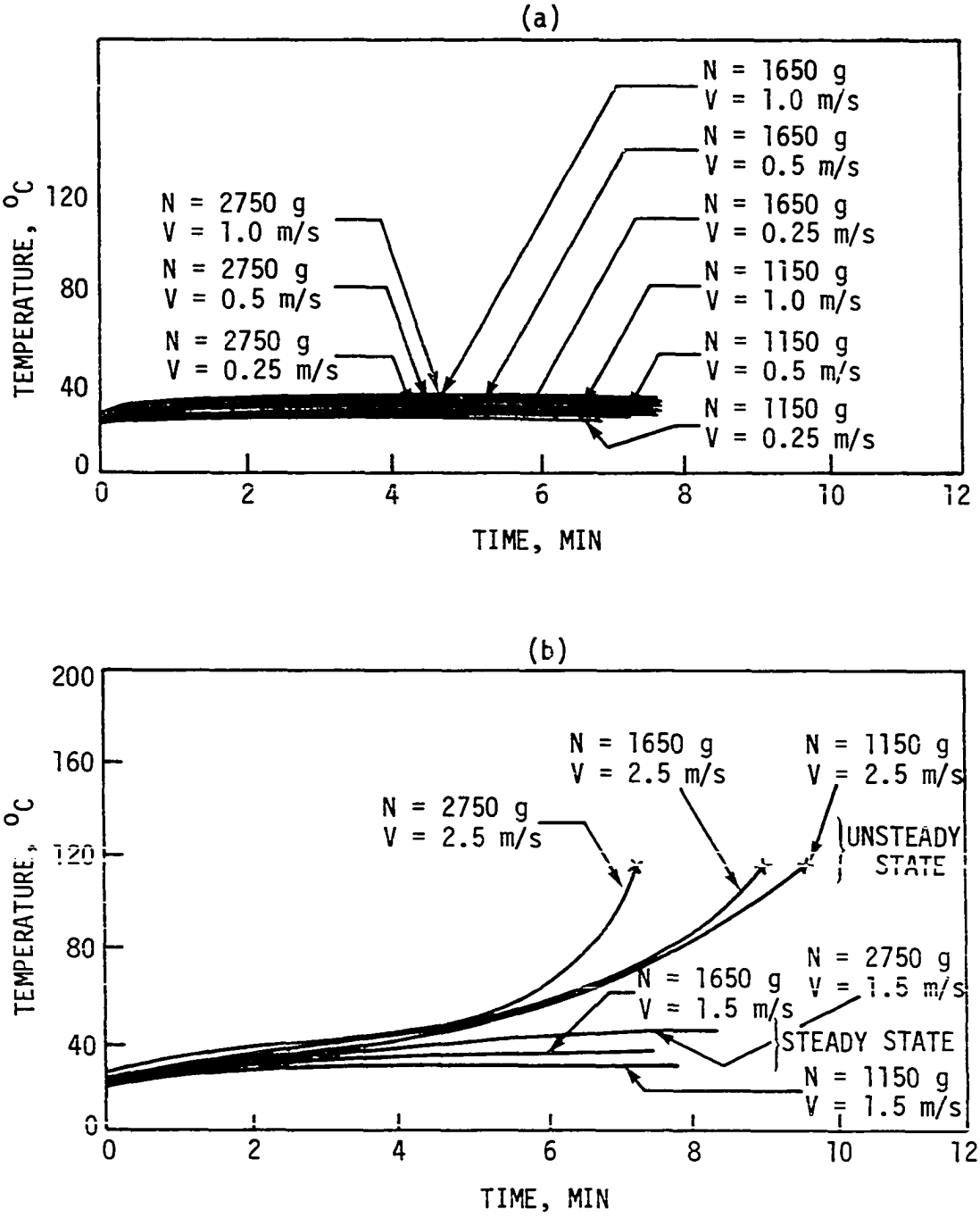

Fig. 6. Plot of temperature vs. time for high density polyethylene; (a) steady state conditions, (b) transition from steady state to unsteady state. x indicates the point of failure.

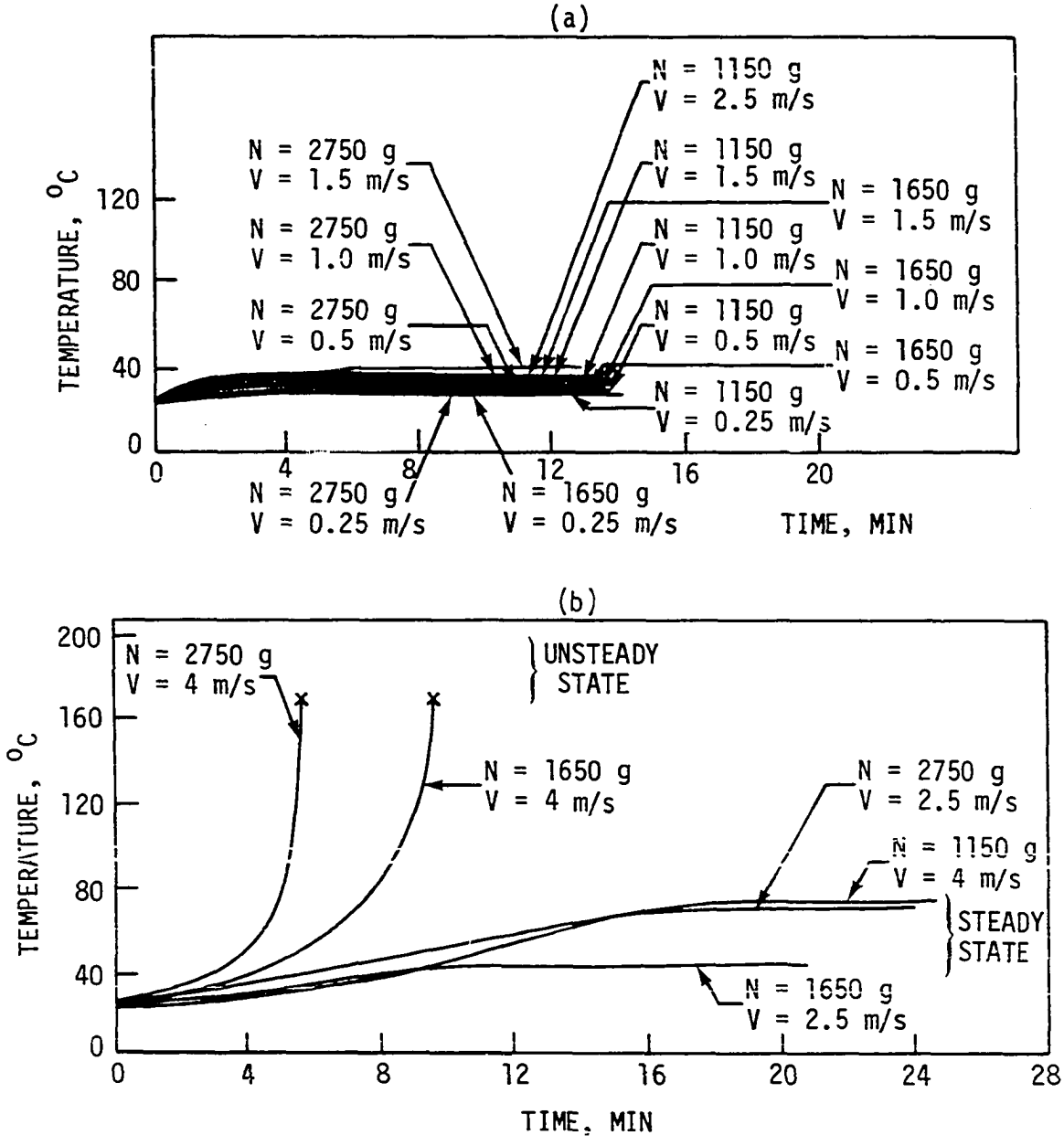

Fig. 7. Plot of temperature vs. time for polyoxymethylene; (a) steady state conditions, (b) transition from steady state to unsteady state. x indicates the point of failure.

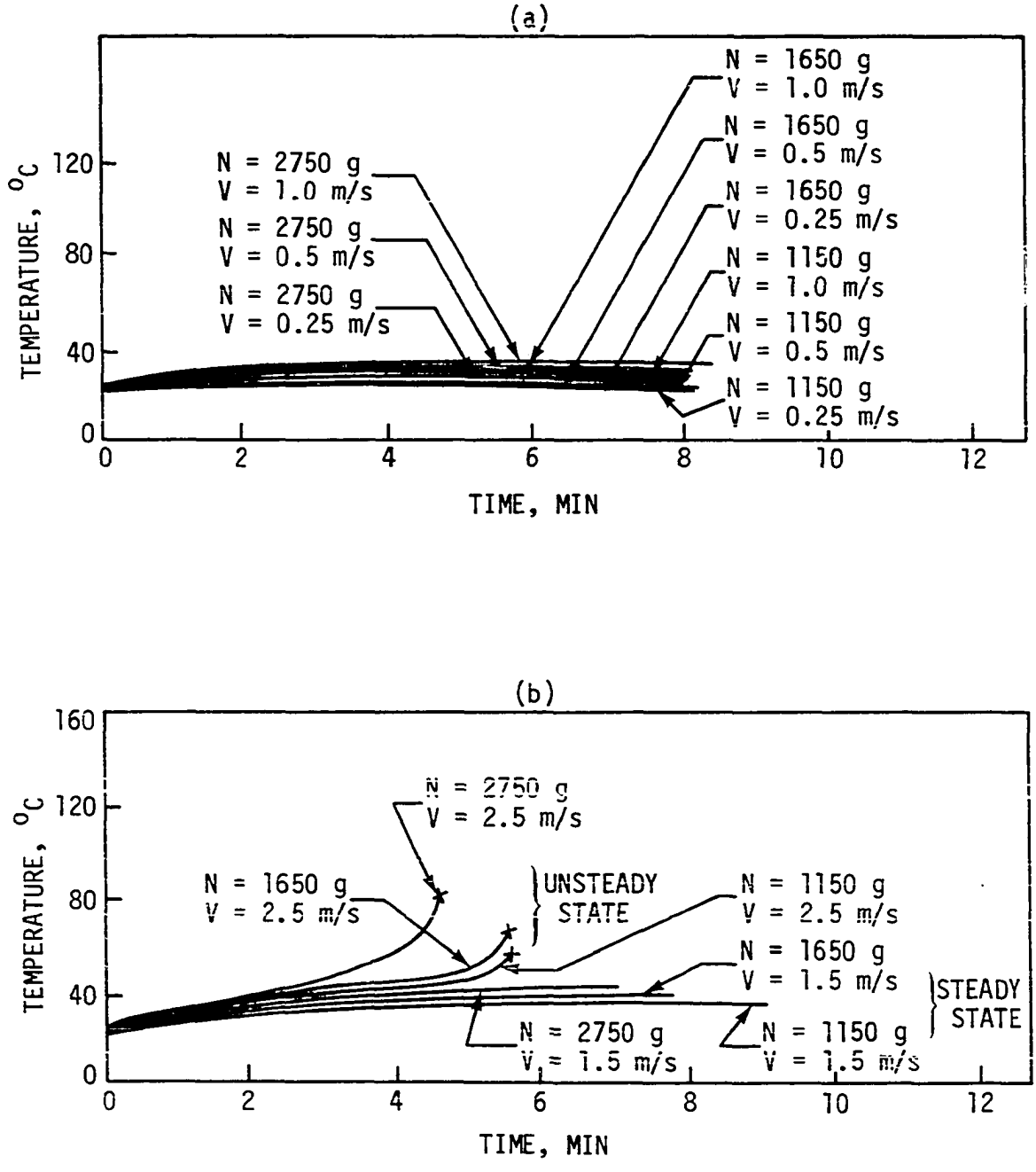

Fig. 8. Plot of temperature vs. time for PTFE; (a) steady state conditions, (b) transition from steady state to unsteady state. x indicates the point of failure.

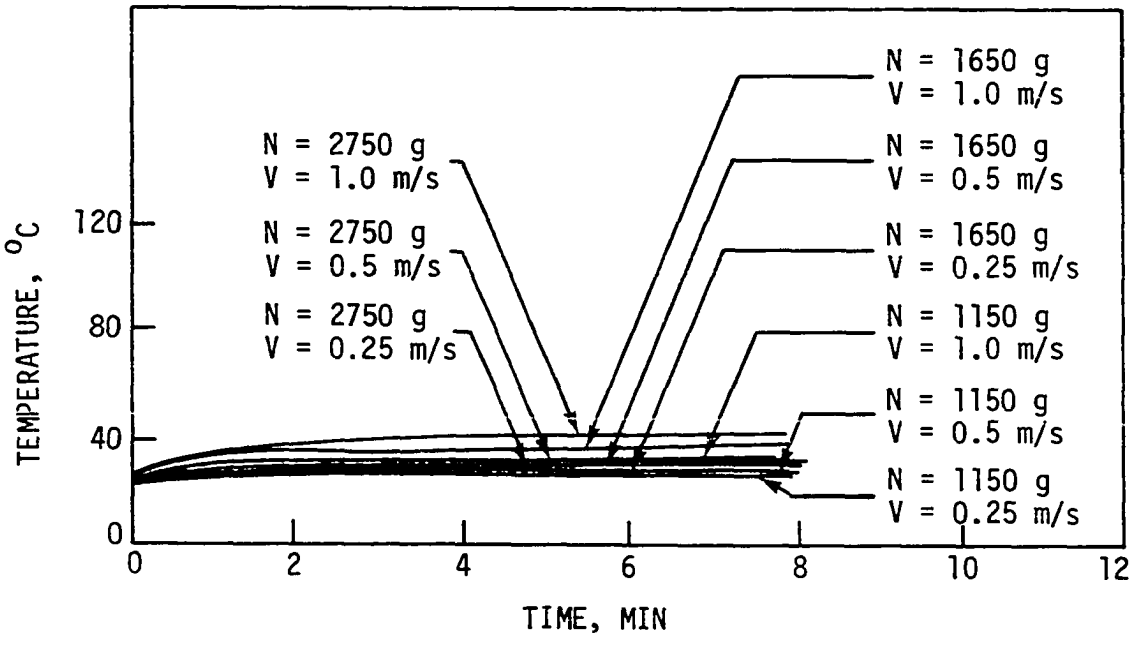

Fig. 9. Plot of temperature vs. time for polypropylene under steady state conditions.

sliding speed range 1.5-2.5 m/sec for high density polyethylene (Figure 6b); 2.5-4 m/sec for polyoxymethylene (Figure 7b); and 1.5-2.5 m/sec for polyoxymethylene (Figure 7b); and 1.5-2.5 m/sec for PTFE (Figure 8b). The failure in the unsteady-state sliding condition for high density polyethylene and polyoxymethylene was accompanied by excessive drawing of fibers in the contact zone and deflection of the pin, creating unstable sliding conditions. The measured temperature at the point of failure for high density polyethylene was about 114°C, and for polyoxymethylene 168°C, both of which are close to the melting points of the respective materials (137°C-142°C for high density polyethylene and 181°C-188°C for polyoxymethylene). The fiber drawing phenomenon is therefore attributed to softening at the contact surface (may be melting at asperity junctions). Contrary to the above two cases, the failure of the PTFE pin was due to excessive wear, leading to unstable sliding conditions, with no sign of fiber drawing or large deflection. The highest measured temperatures in this case were 240°C-280°C, which are considerably lower than the melting point of the material (327°C). As such, no softening (or melting) occurs in the sliding of PTFE.

In order to investigate the cause of excessive deflection, the coefficient of friction vs. time measurements were carried out at one load and sliding speed combination, corresponding to each of the steady state and unsteady state conditions for high density polyethylene, as shown in Figure 10. Whereas the coefficient of friction remains more or less constant in the steady state condition, it increases continuously in the unsteady state condition, rising to a value as high as 4 at the point of failure. Similarly, for polyoxymethylene, the

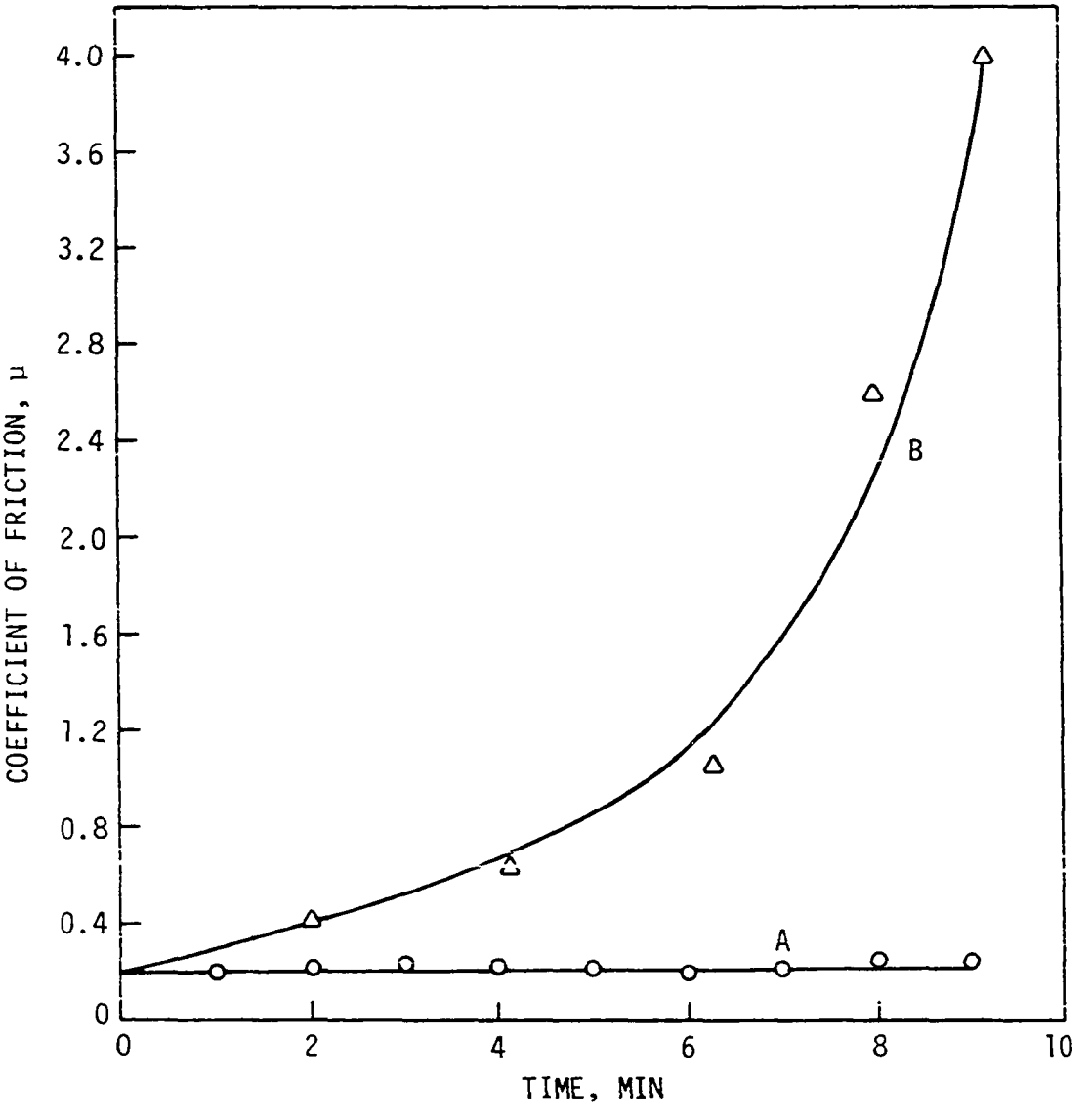

Fig. 10. Plot of coefficient of friction vs. time for high density polyethylene. Curve A for 1150 g load and 0.5 m/sec speed, and curve B for 1150 g load and 2.5 m/sec speed.

coefficient of friction at the point of failure was 4 as opposed to 0.22 in the steady state condition. Thus the excessive deflection is due to a considerable increase in the tangential force at the rubbing surface. A very high value of the coefficient of friction at the failure point results in excessive dissipation of mechanical energy and consequently in a large temperature rise leading to softening. It should be noted that the increase in coefficient of friction and temperature are the two phenomena mutually dependent upon each other. In case of PTFE, there was neither a large increase in temperature nor in coefficient of friction at the point of failure.

4.1.2. Estimation of Heat Transfer Coefficients

In order to calculate the temperature rise at the rubbing surface using Equation (46), the heat transfer coefficients (h for the periphery of the disc and h' for the sides of the disc) need to be estimated. The former is required for the calculation of x_0 and x_n, and the latter for σ. The rotational Reynolds numbers in the present study ranged from about 1,500 (for 0.25 m/sec speed) to 15,000 (for 2.5 m/sec speed). As mentioned earlier, for Reynolds numbers up to about 10,000, Equation (48) is to be used. The problem here is that the Grashof number cannot be calculated unless the temperature rise is known. The effect of the Grashof number on the heat transfer coefficient was, therefore, studied by plotting the right-hand side of Equation (48) as a function of temperature rise both with and without the Grashof number (Figure 11). It was found on calculation that for sliding speeds below 1.0 m/sec, the Grashof number is negligibly small in comparison to $0.5\ Re^2$, because the corresponding temperature rise is very small. As such, a Reynolds number

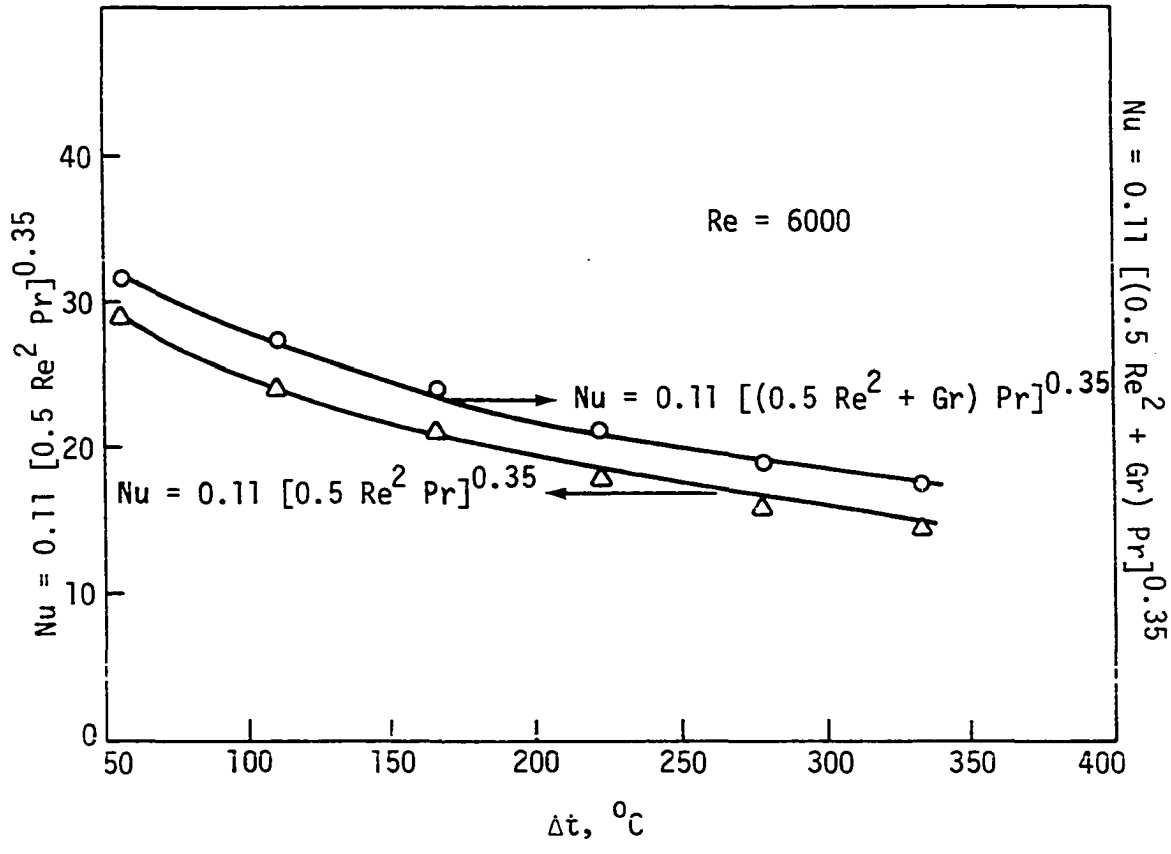

Fig. 11. Plots of temperature rise vs. Nusselt number with and without the Grashof number.

of 6,000, which corresponds to a speed of 1 m/sec, was used for the plot of Figure 11. It can be seen that the Nusselt number values are within 7-20% of where the higher variation corresponds to higher temperature rise. Since the maximum steady state temperature rise was limited to 45°C in our measurements, even for sliding speeds as high as 4 m/sec, the effect of Grashof number on the heat transfer coefficient is insignificant. The following correlation, which is obtained from Equation (48) neglecting the Grashof number, is therefore suggested for calculating the Nusselt number:

$$Nu = 0.11\ (0.5\ Re^2\ Pr)^{0.35} \tag{50}$$

As mentioned in Section 2, the above correlation is valid for Reynolds numbers higher than 10,000 as well.

A critical review of the correlations for heat transfer from a rotating cylinder, proposed by different authors, revealed that the Nusselt number values obtained from these are not significantly different. For example, the following correlation, suggested by Kays and Bjorklund (61), was

$$Nu = 0.095\ Re^{2/3} \tag{51}$$

which gave Nu to be about 6% less than that obtained using Equation (50). This shows that the error, if any, introduced in the estimate of the heat transfer coefficient by ignoring the Grashof number, is close to the experimental variation.

For the calculation of h', Equation (49) may be used. This too involves the Grashof number. Therefore, the effect of the latter on the heat transfer coefficient h' was studied as before by plotting the

calculated values of the Nusselt number, both considering and ignoring the Grashof number as a function of temperature rise (Figure 12). Using the same reasoning as before, it is concluded that the effect of the Grashof number on h' is even more insignificant. Therefore, Equation (49) is reduced to the following:

$$Nu = 0.50\ (Re^2)^{0.25} \tag{52}$$

The properties of air used in estimating the heat transfer coefficients are for the film temperature which is to be calculated. The variation of these with temperature was, therefore, studied as follows. Equation (50) may be written as follows:

$$h \simeq 0.11 \frac{k_a}{D_d} [0.5\ Re^2\ Pr]^{0.35}$$

or

$$\frac{hD_d^{0.3}}{v^{0.7}} = \frac{0.11\ k_a(0.5\ Pr)^{0.35}}{\nu^{0.7}} \tag{53}$$

because $Re = \frac{D_d V}{\nu}$.

The right-hand side of Equation (53) can be evaluated for different temperatures because it contains a Prandtl number (which is a temperature-dependent parameter) and the properties of air. The variation of $[\frac{0.11\ k_a(0.5\ Pr)^{0.35}}{\nu^{0.7}}]$ with temperature is shown in Figure 13.

In a similar manner, Equation (52) may be written as:

(substituting $Re = \frac{VR}{\nu}$)

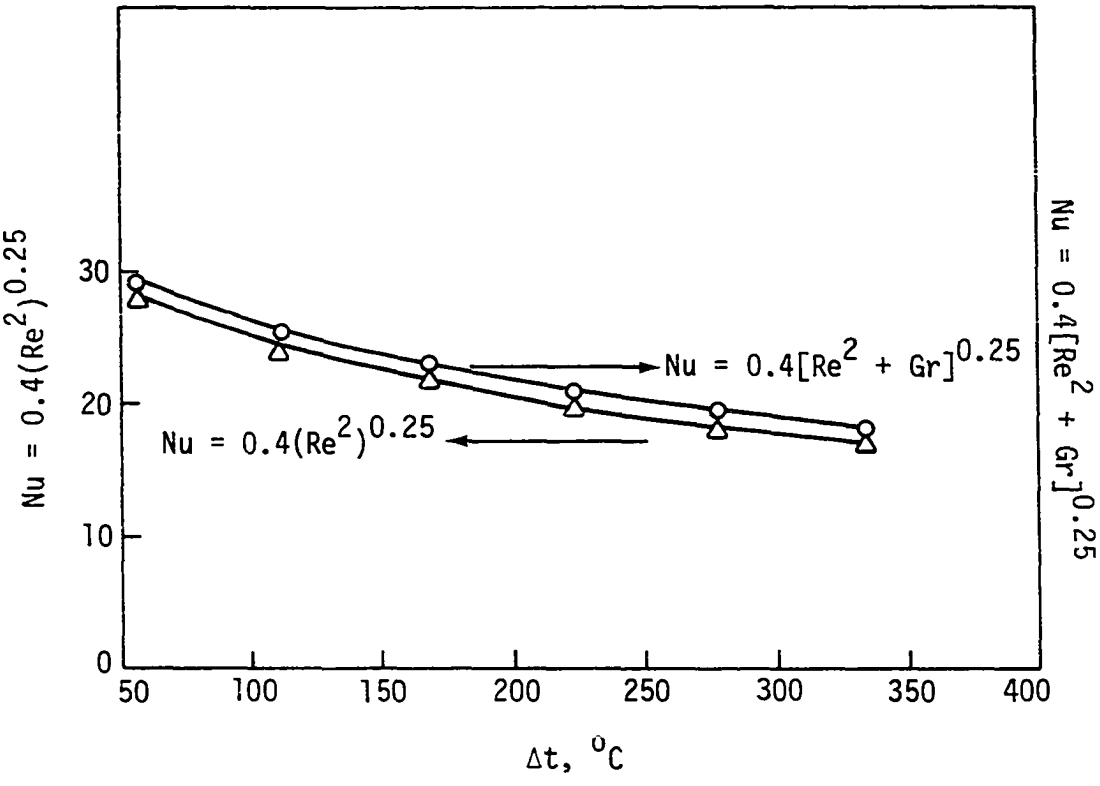

Fig. 12. Plots of temperature rise vs. Nusselt number with and without the Grashof number.

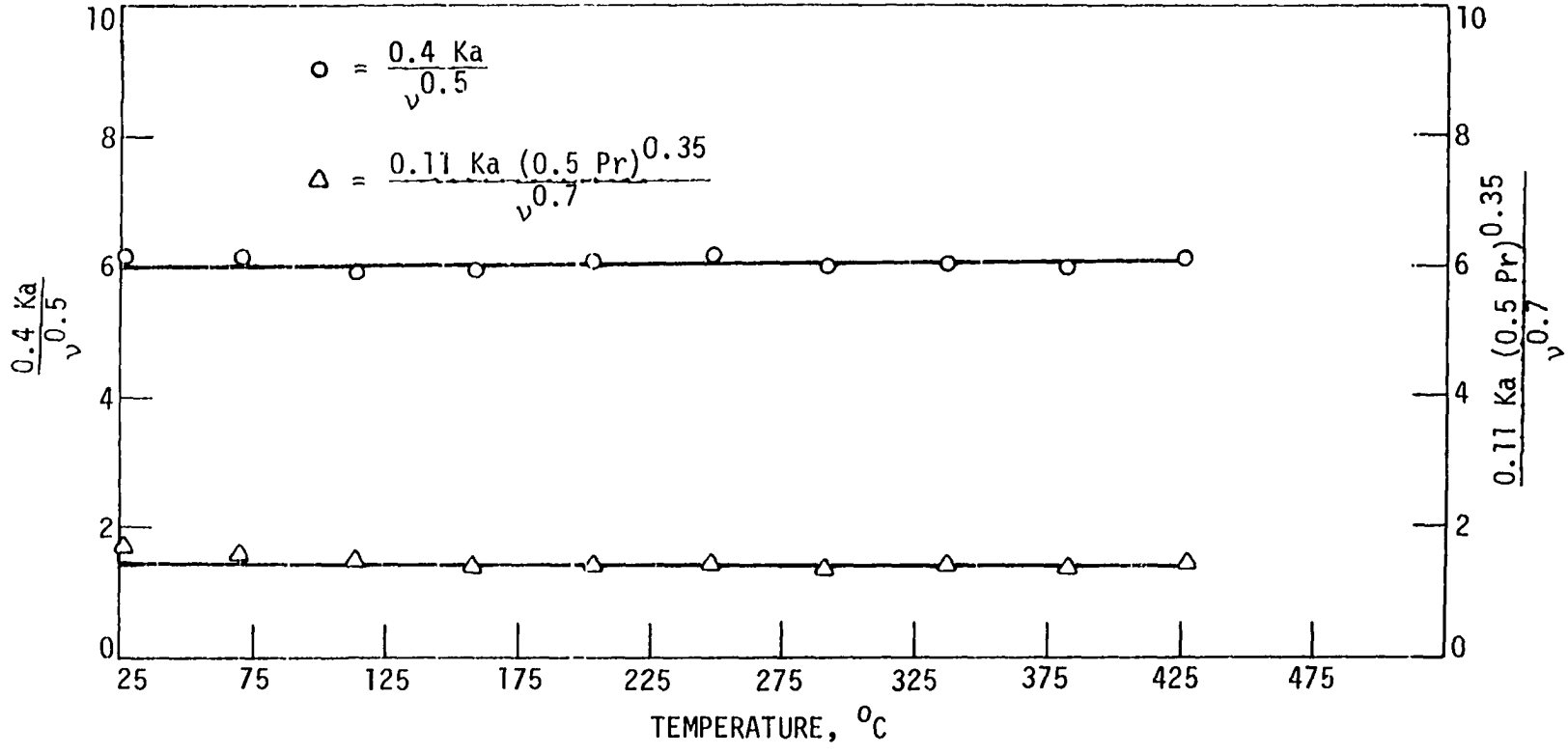

Fig. 13. Variation of $\frac{0.11\ Ka\ (0.5\ Pr)^{0.35}}{\nu^{0.7}}$ and $\frac{0.4\ Ka}{\nu^{0.5}}$ with temperature.

$$h' \left(\frac{k}{V}\right)^{0.5} \simeq \frac{0.40\ k_a}{\nu^{0.5}} \qquad (54)$$

Here too the right-hand side of the above equation can be calculated for different temperatures. It provides the plot of $\left(\frac{0.4\ k_a}{\nu^{0.5}}\right)$ vs. temperature which is also shown in Figure 13.

It is seen from both the plots given in Figure 13 that $\left(\frac{0.4\ k_a}{\nu^{0.5}}\right)$ and $\left(\frac{0.11\ k_a (0.5\ Pr)^{0.35}}{\nu^{0.7}}\right)$ remain fairly constant with temperature. It therefore follows from Equations (53) and (54) that, for all practical purposes, h and h' are also independent of the temperature, because D_d, R and V are constants for any sliding condition. In the calculation of h and h' from Equations (53) and (54), the properties of air corresponding to the ambient temperature may be used without introducing any significant error.

4.1.3. Calculation of Temperature Rise

The temperature rise for steady state conditions was calculated using Equation (46), where γ_1 was obtained from Equation (48). For the maximum variation in sliding speed, which was from 0.25 to 2.5 m/sec, γ_1 was found between 0.97 and 0.99. Neglecting the term $(k_p A_0 N_1 S)$, which is negligibly small compared to the other term $(\pi A' K_d \lambda \tanh N_1)$ in the denominator of Equation (48), γ_1 becomes approximately equal to unity. This will make the predicted temperature rise values larger by about 1-3%, which is satisfactory for normal engineering practice.

The values of the modified Bessel functions of the first and second kind, $I_0(\sigma R)$, $I_n(\sigma R)$, $K_0(\sigma R)$ and $K_n(\sigma R)$, were evaluated for different values of σ with n = 1,2,3...etc., by using the computer programs given in Appendix A. The predicted values of temperature rise along with the

measured values are plotted against the sliding speed for different loads in Figures 14-17 for high density polyethylene, polyoxymethylene, PTFE and polypropylene respectively.

4.1.4. Comparison of the Measured and Predicted Temperature Rise

The comparison between the measured and the predicted values of temperature rise (Figures 14-17) shows that the agreement is as good as can be expected for a complex situation like this. Minor discrepancies are accounted for in terms of an error of $\pm$ 0.5°C in measured temperature rise, created by a narrow spread of the temperature recorder scale. There is also an error in predicted temperature because of the variations in the sliding speed and the coefficient of friction, both of which enter the temperature rise equation.

Considering a variation of 5% in the sliding speed and 10% in the coefficient of friction under apparently identical sliding conditions, a propagation of error analysis was made for the calculated temperature rise. This analysis is given in Appendix B, along with a sample calculation which provides a permissible error of $\pm$1.8°C for polyoxymethylene sliding at 1.5 m/sec and 1650 g load. On the basis of similar calculations, the error in predicted temperature rise was estimated to be $\pm$1.4°C to $\pm$3.4°C, corresponding to the lowest and highest sliding speeds respectively.

4.2. Investigation of Polymer Sliding Surface Using DTA

In order to determine if softening (or melting) of the polymeric pin in the contact region was the basic cause of failure in sliding at speeds higher than 1.5 m/sec, the worn fibrous material, or the material

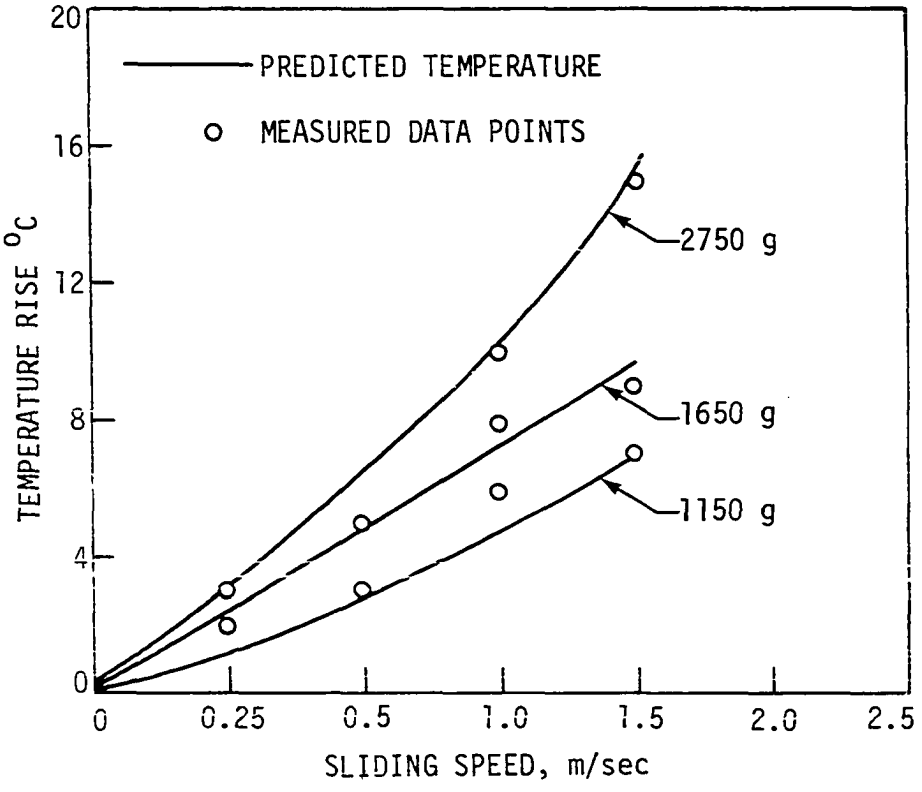

Fig. 14. Temperature rise vs. sliding speed for high density polyethylene pin-steel disc rubbing surface in steady state condition.

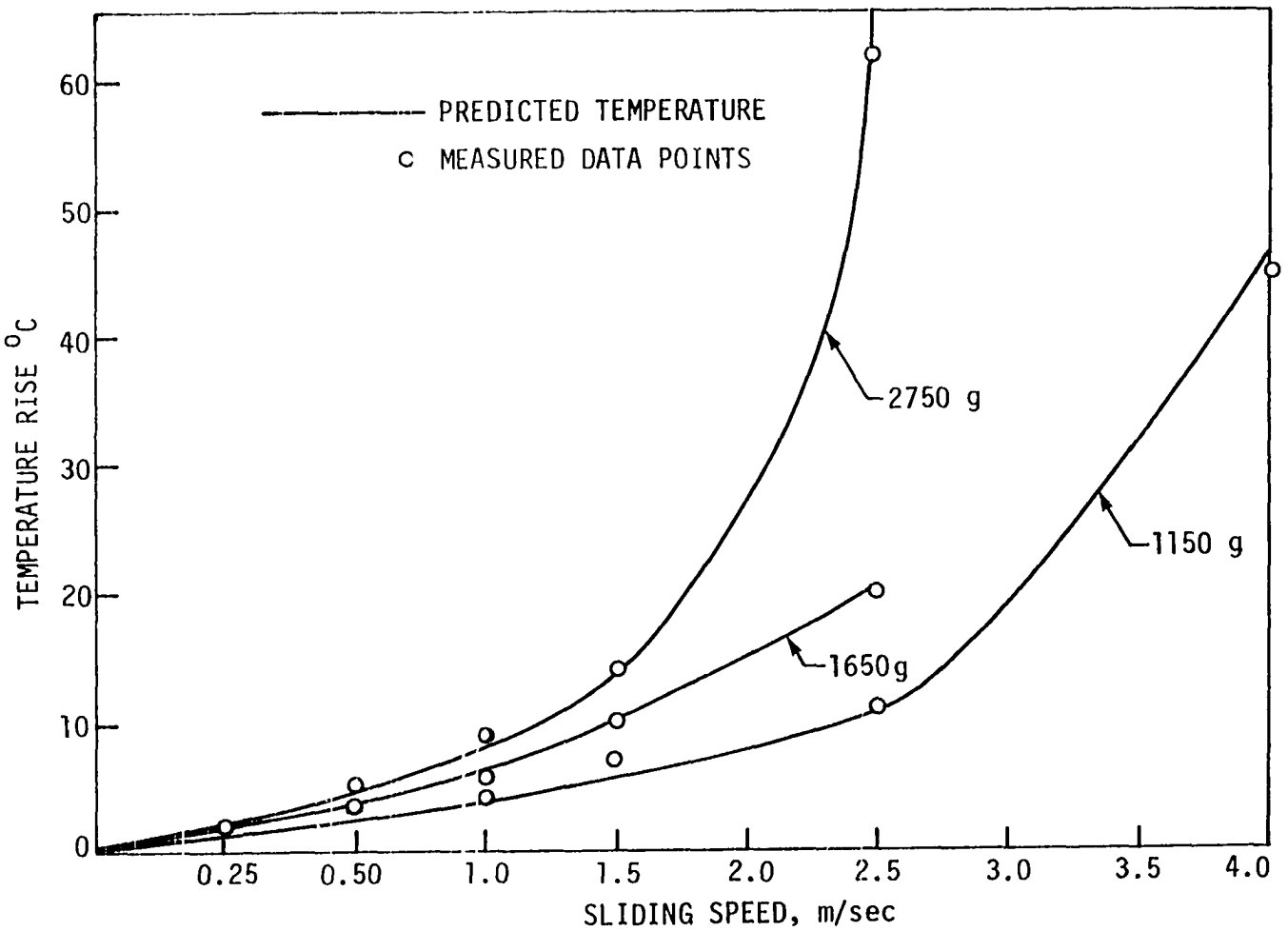

Fig. 15. Temperature rise vs. sliding speed for polyoxymethylene pin-steel disc rubbing surface in steady state condition.

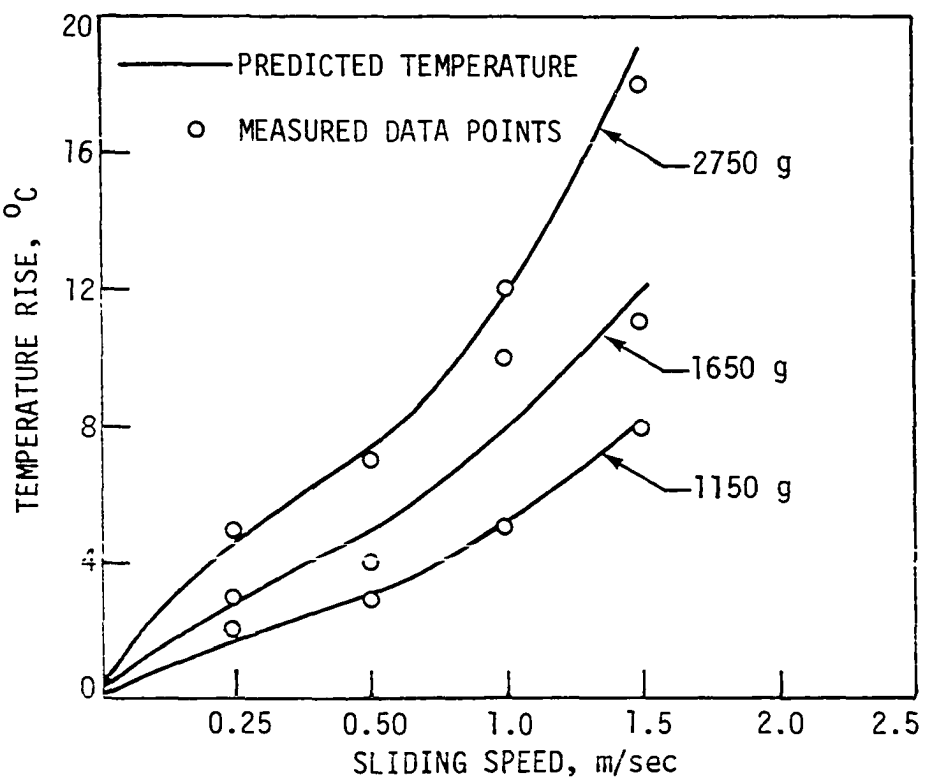

Fig. 16. Temperature rise vs. sliding speed for PTFE pin-steel disc rubbing surface in steady state condition.

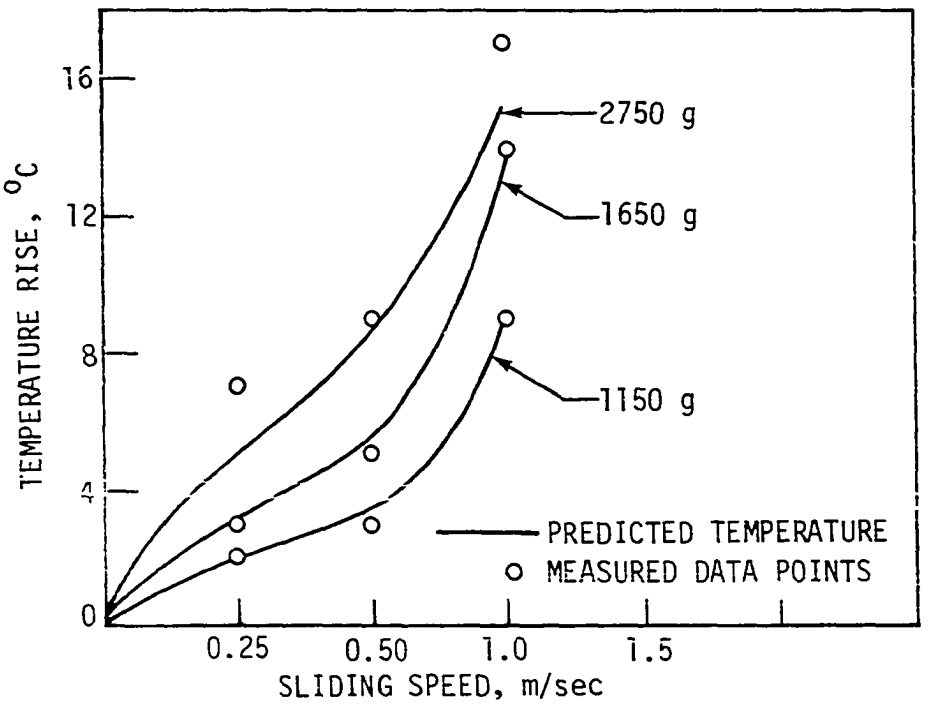

Fig. 17. Temperature rise vs. sliding speed for polypropylene pin-steel disc rubbing surface in steady state condition.

scraped from the rubbing surface of the pin if the fibrous material was not present, was analyzed by DTA. This was done for high density polyethylene, polyoxymethylene and PTFE because the pin failure due to an unsteady state condition was observed only with these materials. Here the sliding speed was varied from 1.5 m/sec to 4 m/sec while the load was kept constant at 2750 g. The DTA results are given in Tables 1-3. A comparison of the melting point of the worn sample with that of the unworn polymer shows that for polyethylene and polyoxymethylene, a lowering in melting point takes place for all the sliding speeds except 1.5 m/sec. Such a lowering in melting point is likely to occur only because of some morphological changes or a result of degradation. Wunderlich and Kashdan (65) have shown by DTA that the melting point of polyethylene was lowered by 1.5^{o}C when the material was melt-annealed at 150^{o}C and cooled rapidly to room temperature. For polyethylene and polyoxymethylene sliding surfaces, similar conditions corresponding to melt-anneal might have been reached at high speeds. When the sliding was stopped, the surfaces cooled quickly; thus, a heating and cooling cycle of this type might have caused morphological changes. The lowering in temperature as a result of degradation was verified by DTA on polyethylene involved in sliding at 2.5 m/sec speed, where the sliding was continued even after the pin had undergone considerable deflection. The rubbing surface was examined in an optical microscope and was found to be covered with a large number of black particles, which were essentially the product of degradation. When this material, together with a thin layer of the underlying material, was analyzed by DTA, a melting point of 138^{o}C was observed. Thus, it could be inferred that under

Table 1. DTA results for high density polyethylene sliding surfaces.[a]

Sliding speed ms^{-1}	Specimen weight g	Melting point ^{o}C
1.5	0.0113	142
2.5	0.0126	138
4	0.0133	136

[a]The load was kept constant at 2750 g. The melting point of the unworn polyethylene as measured by DTA was 142°C.

Table 2. DTA results for polyoxymethylene sliding surfaces.[a]

Sliding speed ms^{-1}	Specimen weight g	Melting point ^{o}C
1.5	0.0135	188
2.5	0.0128	186
4	0.0115	185

[a]The load was kept constant at 2750 g. The melting point of unworn polyoxymethylene as measured by DTA was 188°C.

Table 3. DTA results for PTFE sliding surfaces.[a]

Sliding speed ms^{-1}	Specimen weight g	Melting point ^{o}C
1.5	0.0112	327
2.5	0.0108	327
4	0.0120	327

[a]The load was kept constant at 2750 g. The melting point of the unworn PTFE as measured by DTA was 327°C.

severe sliding conditions (here 2.5 and 4 m s^{-1} speed conditions), the polymeric material is being heated to a temperature equal to or at least close to the melting point, and may also be degraded at some asperity junctions.

The DTA results are in agreement with the temperature measurement studies on high density polyethylene and polyoxymethylene at sliding speeds higher than 1.5 m/sec, where the temperature reached at the point of failure was close to the melting point of the respective material. The only disagreement between the two studies is for polyoxymethylene sliding at 2.5 m/sec speed and 2750 g load, where the DTA provided evidence of softening when the measured temperature was well-below the melting point of the polymer. Since these measurements provide an estimate of the average temperature rise, such a disparity is not ruled out.

As seen in Table 3, the melting point of PTFE for any of the sliding conditions is not lowered. Therefore, it is reasonable to conclude that melting did not take place at the sliding surface of PTFE even at higher sliding speeds. This is in agreement with the temperature measurement studies, because the measured temperatures were 240-280^{o}C below the melting point of the material.

4.3. Examination of Polymer Sliding Surfaces by Scanning and Transmission Electron Microscopy

4.3.1. Scanning Electron Microscopy

The sliding surfaces of high density polyethylene, polyoxmethylene and PTFE were examined by scanning electron microscopy to verify the

conclusions derived from DTA studies and to gain some further insight into the nature of wear phenomenon. The sliding was performed under a constant load of 2750 g and at three speeds, namely, 1.5, 2.5 and 4.0 m/sec. The sliding conditions and the materials selected were the same as those used earlier in DTA studies.

The scanning electron micrographs of sliding surfaces of the three polymers mentioned above are shown in Figures 18-22. It is seen that the appearance of these surfaces differs with varying sliding conditions. When sliding was performed at a speed of 1.5 m/sec, the surfaces of all the three materials exhibited abrasion marks along with polymer wear particles or their agglomerations (Figure 18). The abrasion marks in the case of PTFE are covered with a large number of wear particles because of the severe wear of this material. At the higher speed of 2.5 m/sec, the deformation of sliding surfaces in the form of a localized flow of material is indicated for high density polyethylene and polyoxymethylene in Figures 19(a) and 19(b), respectively. The flow is in the direction of sliding and has probably been caused by thermal softening of the rubbing surfaces. No such material flow was observed on the sliding surfaces of these two polymers at the lower speed of 1.5 m/sec. At the higher speed of 4 m/sec, the localized flow of materials on the sliding surfaces of polyethylene and polyoxymethylene is seen even more clearly in Figure 20(a,b). A similar flow of material has been reported by Tanaka and Uchiyama (32) on the sliding surfaces of polypropylene and nylon at 1 m/sec speed. The localized flow of material is much more obvious in the micrograph of the polyoxymethylene sliding surface obtained at a higher magnification (Figure 21).

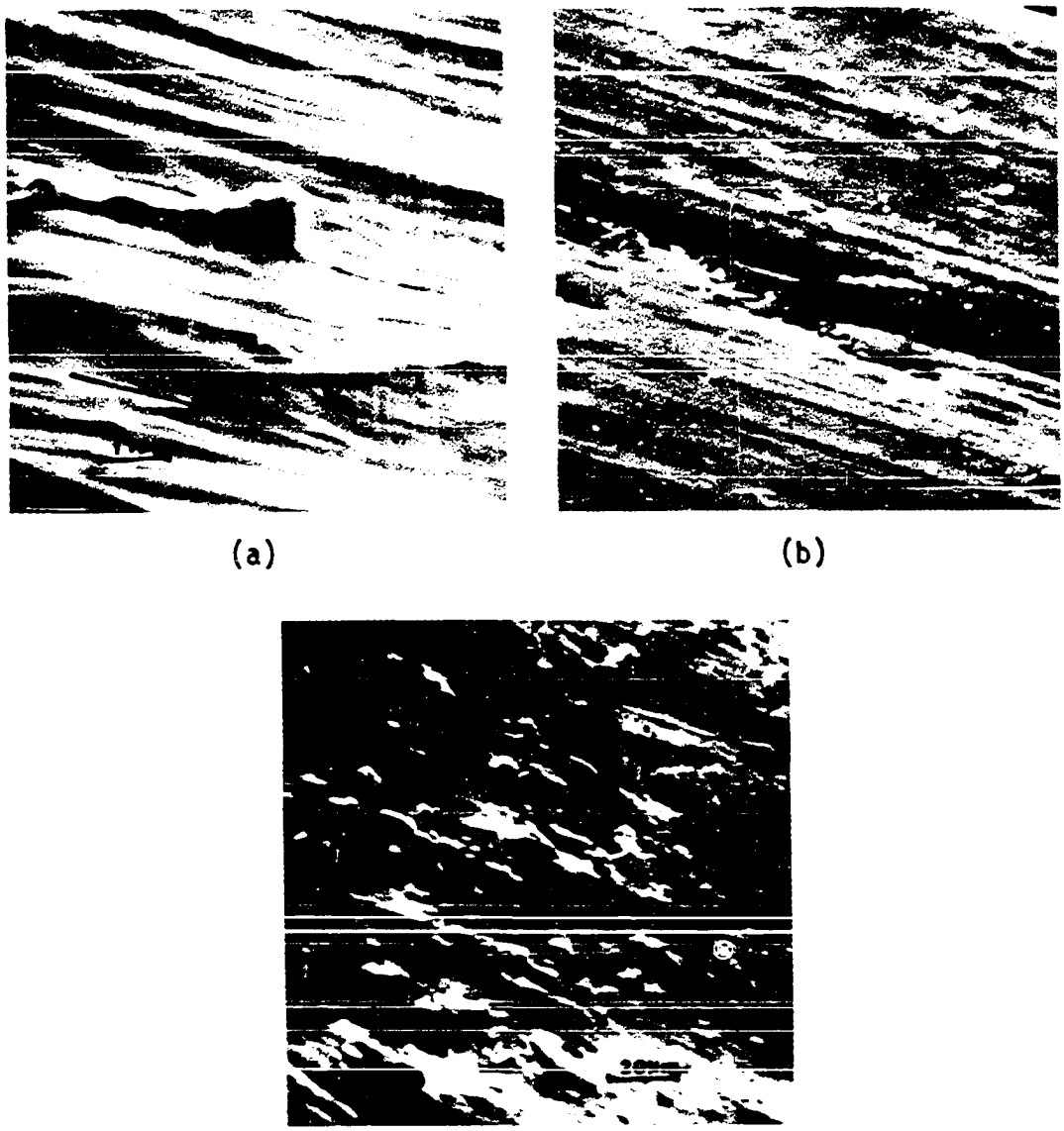

Fig. 18. Scanning electron micrographs of polymer sliding surfaces: (a) high density polyethylene; (b) polyoxymethylene; (c) PTFE. Sliding conditions: speed 1.5 m/sec, load 2750 g. The direction of sliding is shown by the arrow.

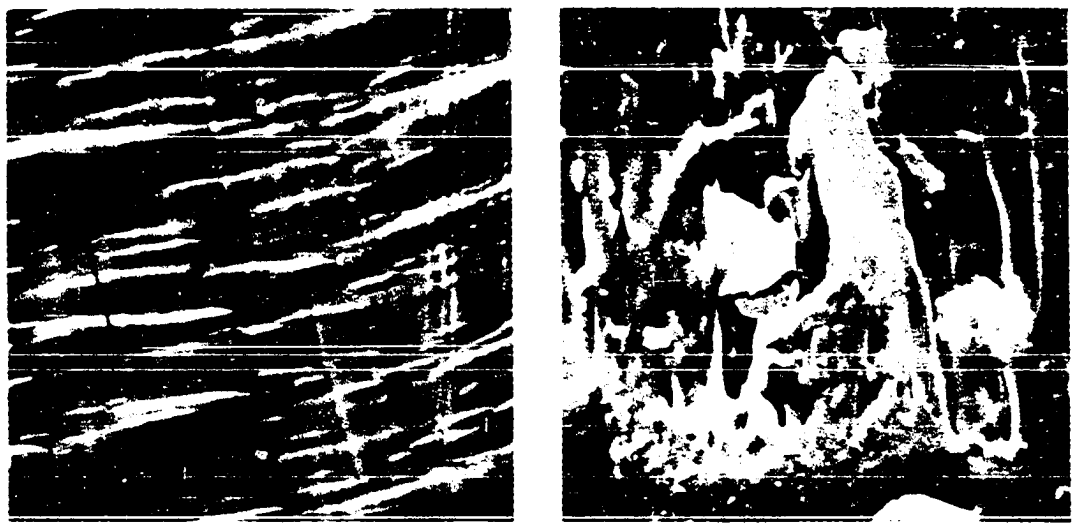

(a) (b)

Fig. 19. Scanning electron micrographs of polymer sliding surfaces showing localized flow of material in the direction of sliding (shown by the arrow): (a) high density polyethylene; (b) polyoxymethylene. Sliding conditions: speed 2.5 m/sec, load 2750 g.

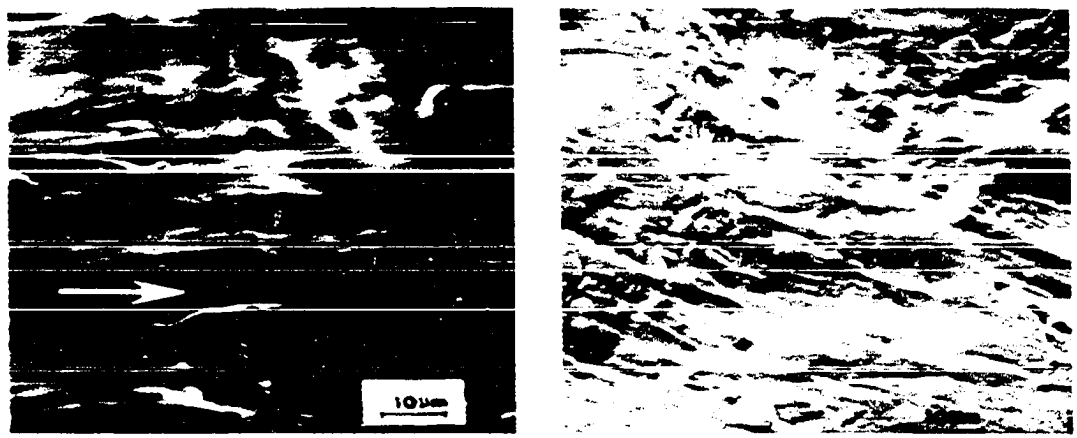

(a) (b)

Fig. 20. Scanning electron micrographs of polymer sliding surfaces: (a) high density polyethylene; (b) polyoxymethylene. Sliding conditions: speed 4 m/sec, load 2750 g. The sliding direction is shown by the arrow.

Fig. 21. Scanning electron micrograph of polyoxymethylene sliding surface showing the flow of material in the direction of sliding (shown by the arrow). Sliding conditions: same as in Fig. 20.

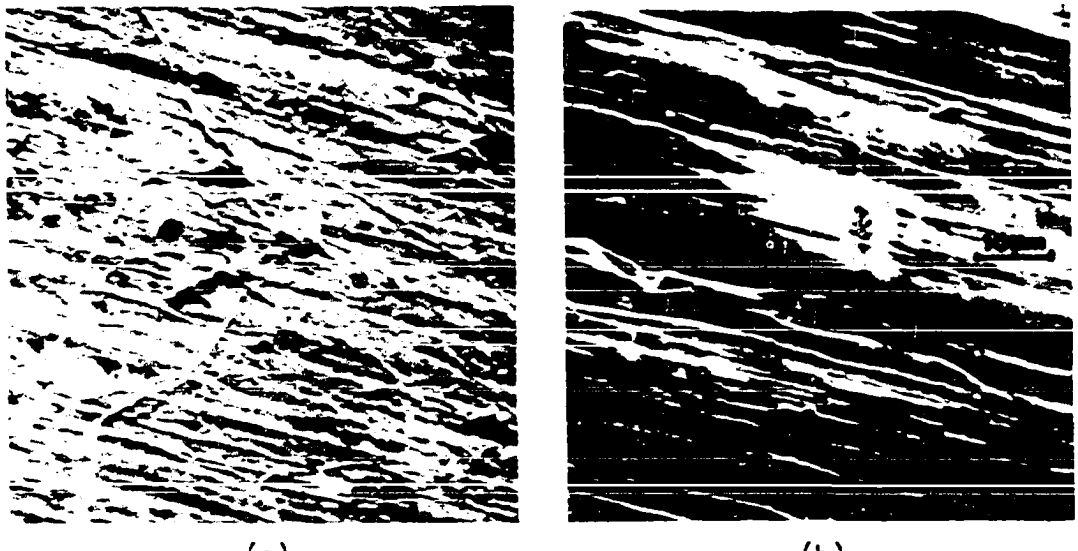

Fig. 22. Scanning electron micrographs of PTFE sliding surface. Sliding conditions: (a) speed 2.5 m/sec, load 2750 g; (b) speed 4 m/sec, load 2750 g. The sliding direction is shown by the arrow.

The scanning electron micrographs of PTFE sliding surfaces showed that the appearance of these surfaces was different from that of the other two polymers, where sliding was performed at the speeds of 2.5 and 4 m/sec (Figure 22). Here no localized flow of material is indicated, although some discrete lumps of wear fragments are seen on the surfaces. The fibers and films observed on these surfaces are typical of the worn surface of PTFE, as reported by Tanaka et al. (30). The absence of material flow here verifies that softening (or melting) does not take place in the case of PTFE even at high speeds.

The comparison of these results with those obtained by DTA supports our finding that softening (or melting) is the cause of catastrophic wear for high density polyethylene and polyoxymethylene at the sliding speeds of 2.5 and 4 m/sec. This is not the case with PTFE, and the excessive wear of this material is due to the continuous removal of the transferred material from the interface. The reason for this is the much poorer adhesion of PTFE in comparison to that of the other polymeric materials.

4.3.2. Transmission Electron Microscopy

In order to ascertain the probable mechanism of wear at very low sliding speeds, single-stage replicas of the sliding surfaces of PTFE, high density polyethylene, polyoxymethylene, polypropylene and polycarbonate were made. These were examined in a transmission electron microscope, and the micrographs are given in Figures 23-28. The arrow shows the direction of sliding.

By examining the micrographs from two different locations of PTFE sliding surfaces (Figures 23, 24), it can be seen that a large number

Fig. 23. Transmission electron micrograph of PTFE sliding surface and electron diffraction pattern from the encircled portion in the top-left corner. Sliding conditions: speed 0.002 m/sec, load 1600 g, time 20 min.

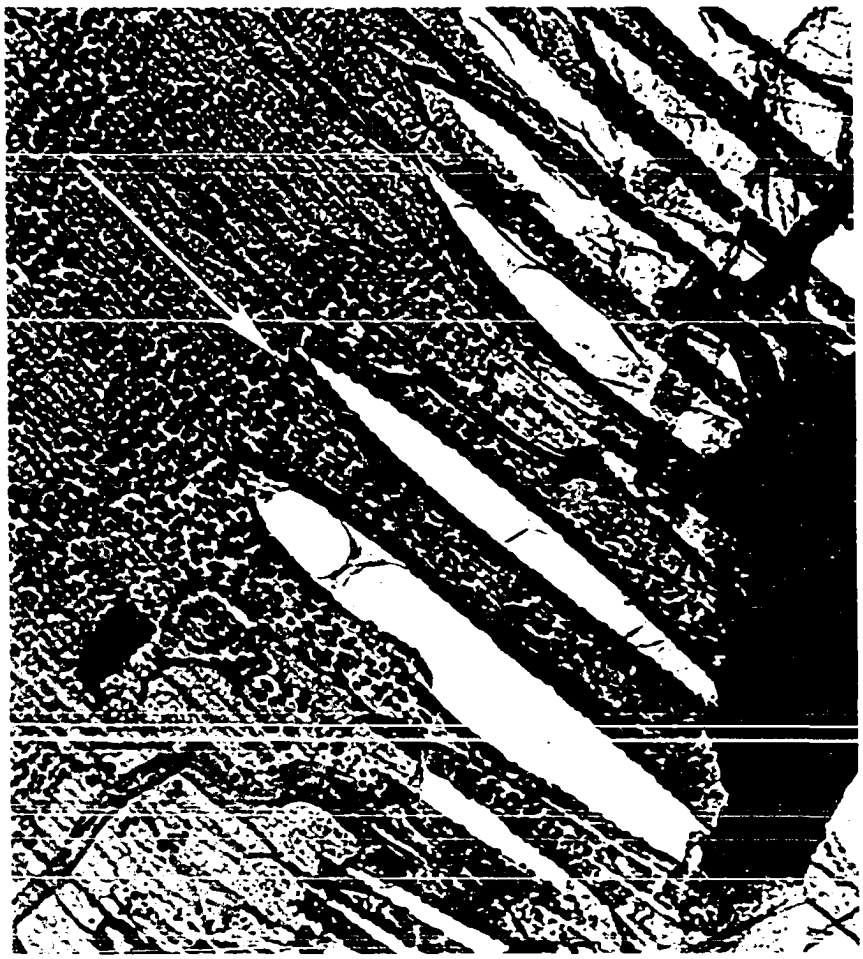

Fig. 24. Transmission electron micrograph of the same sliding surface as in Fig. 23, but from a different location.

of thin films are stretched across an abrasion groove. A selected area electron diffraction pattern, obtained from the encircled location in Figure 23, is also inserted in the figure. The interplanar distances were found by calculation to be 1.94, 1.62, 1.46 and 1.29 Å. These d-spacings agree within the limits of experimental error with the x-ray results of PTFE by Bunn and Howells (66), and correspond to the diffraction from planes (0010), (300), (306) and (0015), respectively (a sample calculation is given in Appendix C). Thus it is possible to say conclusively that these are films of the PTFE material. The sharpness of the diffraction spots indicates that the films are highly oriented. From the positions of the layer lines, it was found that the c-axis has been oriented in the direction of sliding. The thickness of these films (estimated from the curled edges) is approximately 300 Å, which is roughly equal to the lamellar thickness of a polymeric material. Thus, the mechanism of the film formation during the sliding process at low speeds for PTFE is interlamellar shear, which is in agreement with the explanation provided by Makinson and Tabor (23) and Speerschneider and Li (67). Tanaka et al. (30) have pointed out that these films are produced because of the deformation and destruction of its characteristic banded structure.

Similar to the case of PTFE, thin films stretched across an abrasion groove are seen even in the micrographs of the materials, namely, high density polyethylene, polyoxymethylene and polypropylene (Figures 25, 26 and 27). In case of polyethylene (Figure 25), the films are not drawn as neatly and profusely as they are for PTFE (Figures 23 and 24). The analysis of the diffraction pattern obtained from polyethylene film showed

Fig. 25. Transmission electron micrograph of high density polyethylene sliding surface and electron diffraction pattern from the encircled portion in the top-left corner. Sliding conditions: Same as in Fig. 23.

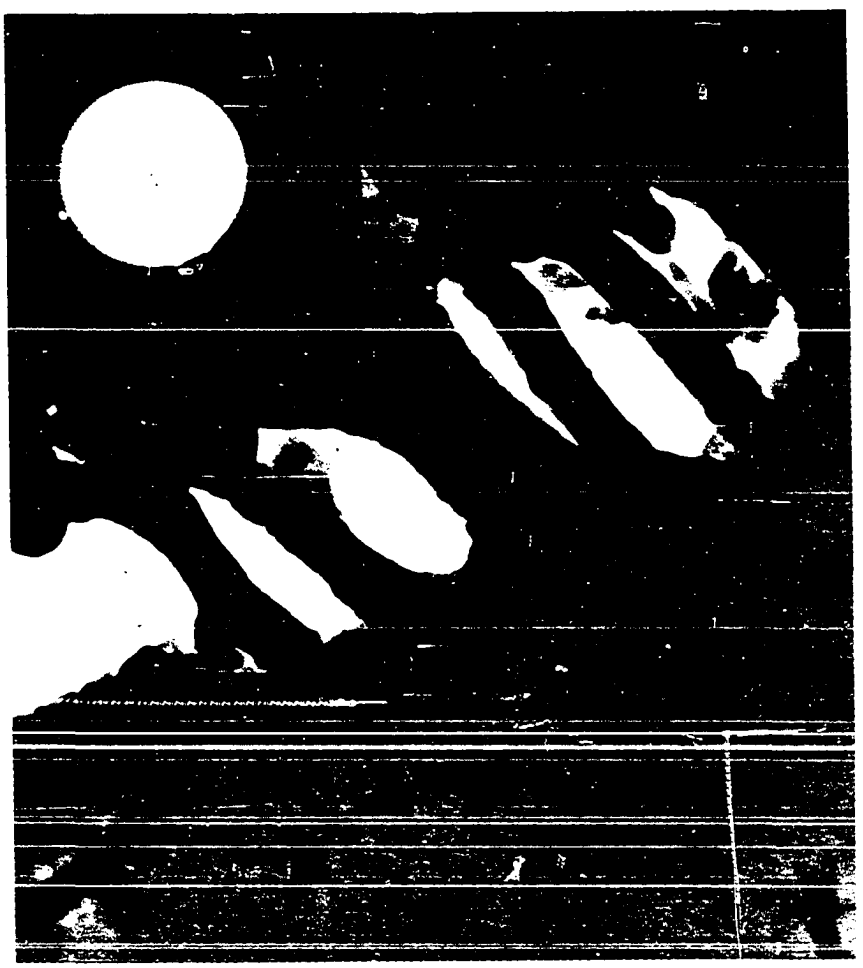

Fig. 26. Transmission electron micrograph of polyoxymethylene sliding surface and electron diffraction pattern from the encircled portion in the top-left corner. Sliding conditions: Same as in Fig. 23.

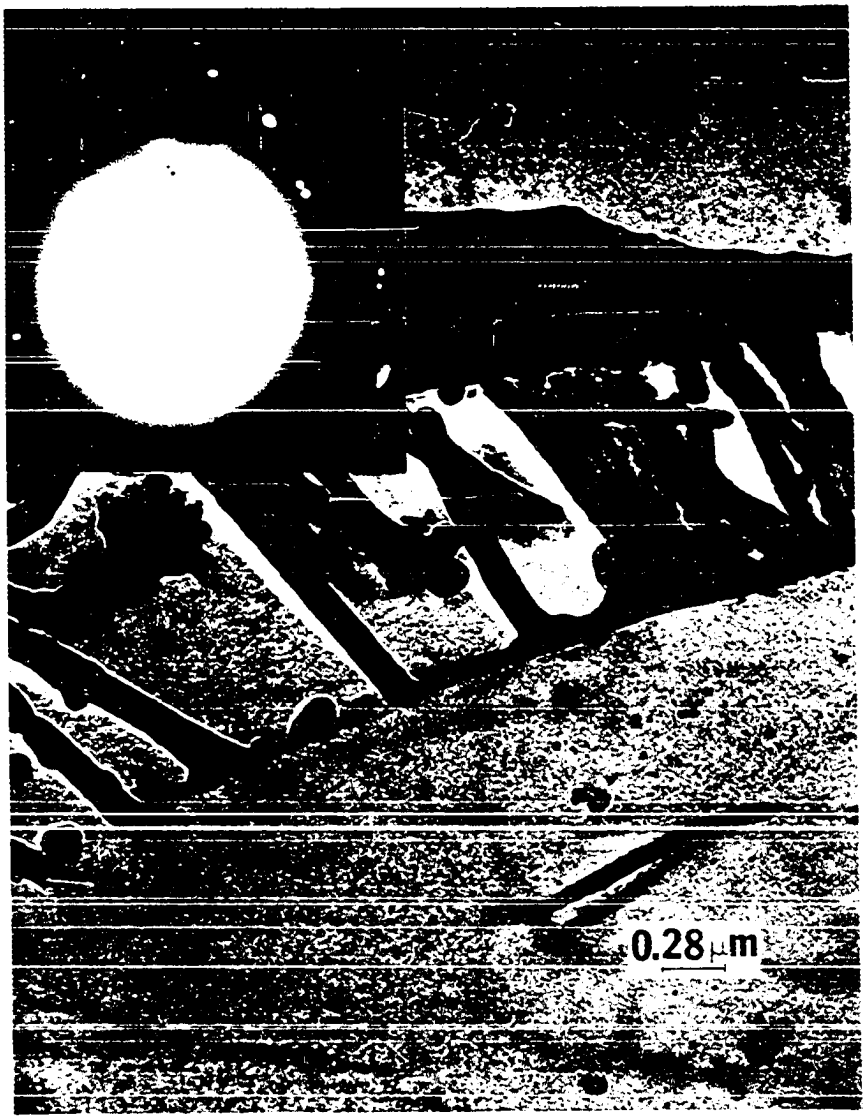

Fig. 27. Transmission electron micrograph of polypropylene sliding surface and electron diffraction pattern from the encircled portion in the top-left corner. Sliding conditions: Same as in Fig. 23.

diffraction from planes (111), (211), (400), (230) and (330), which are in agreement with those reported by Bunn (68). Here again the c-axis was found to be oriented in the direction of sliding. Briscoe et al. (31) and Tanaka and Miyata (33) have also observed films on the sliding surface of high density polyethylene, but they did not identify these. The analysis of the diffraction pattern, obtained from the film stretched across an abrasion groove (Figure 26) as in the case of sliding on a polyoxymethylene surface, provided diffraction from planes (100), (110) and (205), corresponding to the inner three circles of the spots. These diffracting planes have been observed by Uchida and Tadokoro (69) and Bahadur (70) for polyoxymethylene in x-ray analysis. Thus, it was concluded that these are polyoxymethylene films resulting from the shearing action occurring at the interface during sliding. The films were estimated to have a thickness comparable to that of PTFE. Thin films were observed even on the abraded surface of polypropylene and the diffraction pattern was obtained from the film in the encircled location (Figure 27).

The indexing of the diffraction pattern for isotactic polypropylene (71), was performed considering a monoclinic crystal structure because the monoclinic form is more common than the hexagonal form. With increasing diameters of diffraction spots the corresponding planes are (110), (130), (041), (150), (060) and (200). The diffraction from these planes has been reported for polypropylene by Binsberger and DeLange (72) and Bahadur (73).

Contrary to the results obtained for PTFE, polyethylene, polyoxymethylene and polypropylene, films stretching across the abrasion grooves could not be observed when the replicas of the polycarbonate (Bisphenol-A)

sliding surface were examined in a transmission electron microscope. However, fragmented films appear to be scattered around on the surface (Figure 28). The electron diffraction pattern, shown in a corner of the micrograph, was obtained from one of these films.

The appearance of diffraction spots from an amorphous polymer may raise some questions. Research in recent years on the morphology of amorphous polymers has shown, however, that these polymers consist of small domains (about 30-100 Å) with local order within them. These domains are often referred to as the nodular structure in an amorphous polymer (74). The random coil structure concept used to explain the morphological structure of amorphous polymers in the past is losing ground rapidly. To date, nodular structure has been observed in several polymers, namely, polycarbonate, poly(ethylene terepthalate), natural rubber, isotactic and atactic polystyrene and poly(methyl methacrylate) (74, 75). It is possible that severe deformation at the polymer sliding surface orients these locally-ordered regions of nodules, thereby creating an induced crystal structure. If this is so, an oriented diffraction pattern would be expected for polycarbonate as well. Yeh and Geil (76) observed that when a thin film of poly(ethylene terepthalate) was stretched (drawn), the nodules aligned themselves in short rows in the direction they were drawn. The electron diffraction pattern from such a film indicated that a three-dimensional crystal structure had developed. This type of induced crystallinity due to deformation has also been observed in polyisobutylene (77) and natural rubber (78-80).

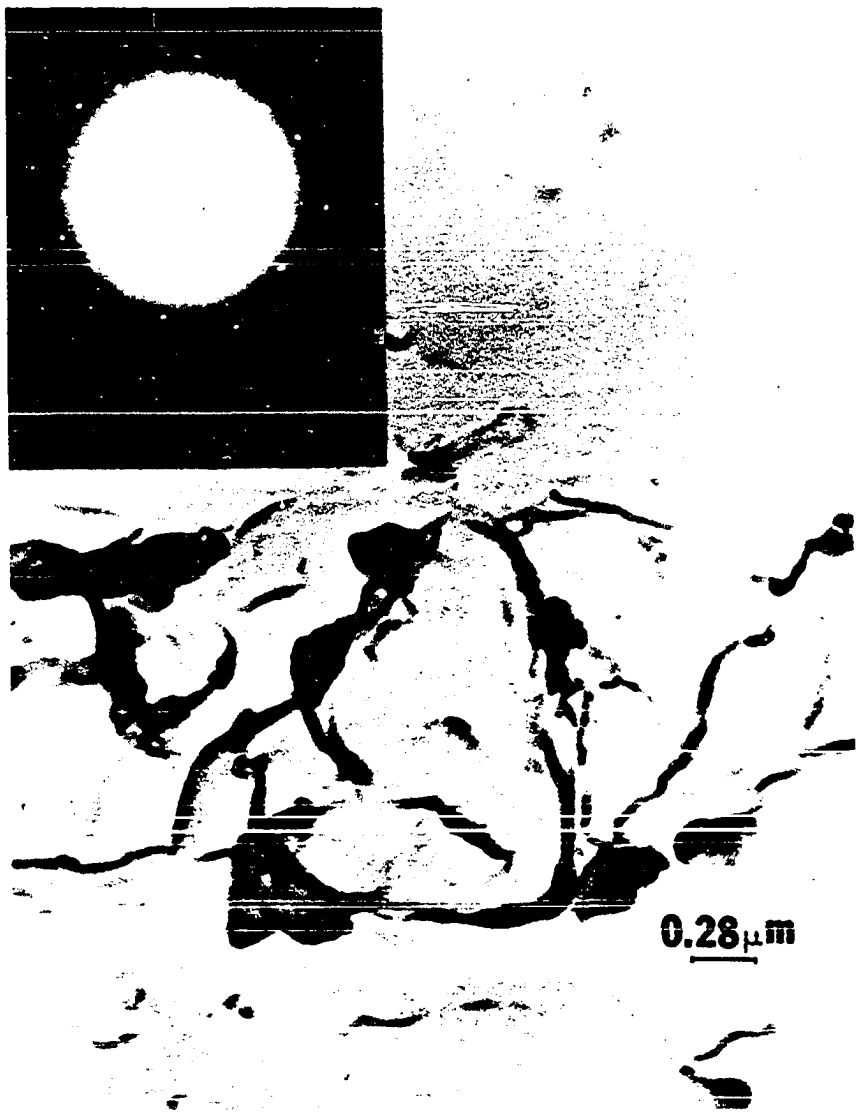

Fig. 28. Transmission electron micrograph of polycarbonate sliding surface showing fragmented films and electron diffraction pattern from one such film in the top-left corner. Sliding conditions: Same as in Fig. 23.

4.4. Wear Particle Analysis

4.4.1. Measurement of Particle Size

An analysis of loose wear fragments was performed in order to develop a better understanding of wear in general. The microscopic examination revealed that the shape of the particles resembled that of a flattened ellipsoid. This is in agreement with the observations of Rabinowicz (40) and Soda et al. (41) on the wear fragments of metallic materials in adhesive wear situations. The size of wear particles was measured along the major and minor axes of the elliptical surface, using an optical microscope under the load conditions mentioned in experimental section (Section 3). From the data obtained, histograms (Figures 29-32) were plotted with the elliptical surface area of particles as the abscissa and the number of occurrences as the ordinate. It may be seen from these histograms that the surface area (or size) of wear particles has more or less the same distribution, irrespective of the load. This is shown in Table 4 where the surface area ranges have been given, ignoring occurrences up to 5. It may also be noted that the surface area of PTFE particles is much larger than that of the other polymers; this supports the higher wear rate of PTFE, which is so commonly reported in the literature.

4.4.2. Estimation of Wear Particle Thickness

The thickness of wear particles has been estimated considering the following model for the formation of a wear particle. When the asperities on sliding surfaces come in contact, an adhesive junction is formed. The latter is subjected to a compressive stress due to normal load and a shear stress because of the relative motion, as shown in

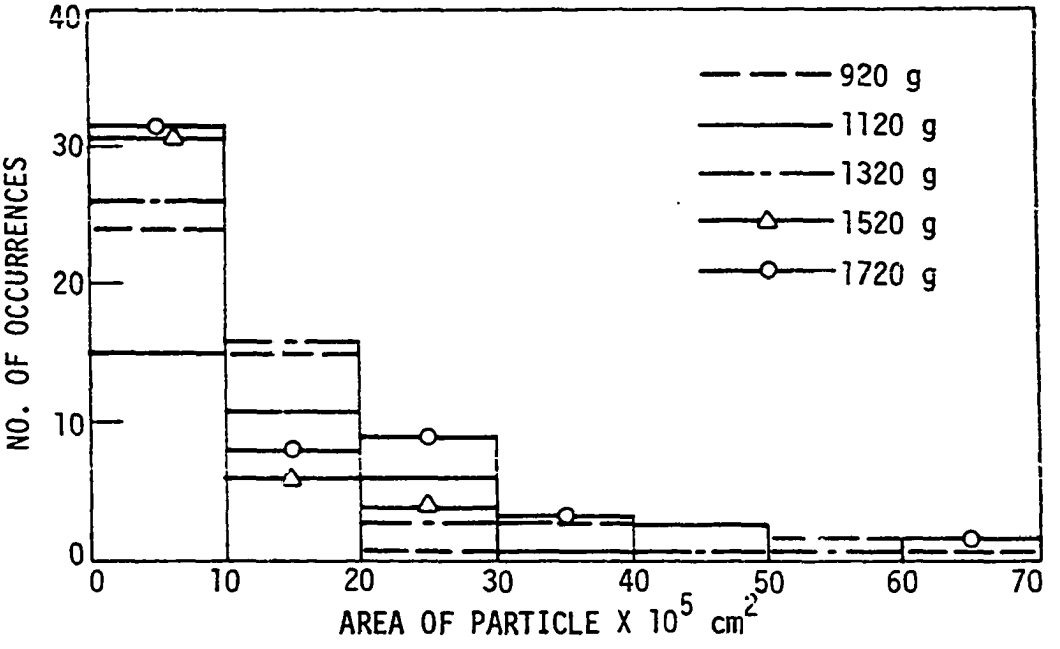

Fig. 29. Histogram of wear particle area for high density polyethylene. Sliding conditions: speed 0.5 m/sec, time 1 hr.

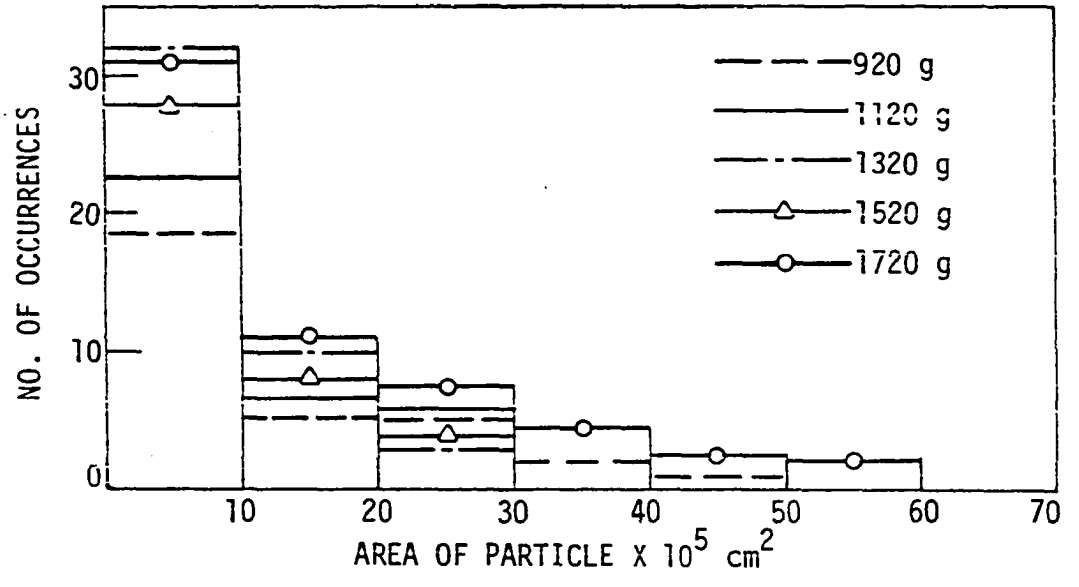

Fig. 30. Histogram of wear particle area for polyoxymethylene. Sliding conditions: same as in fig. 29.

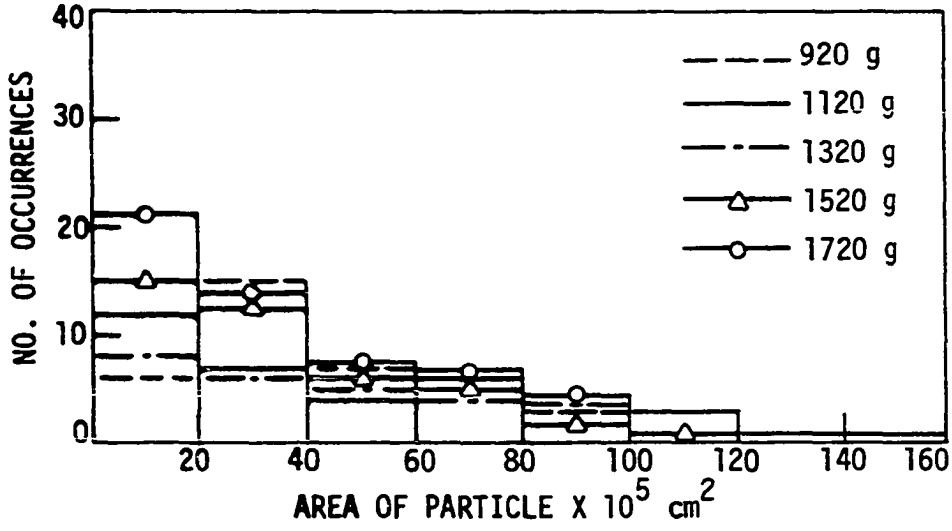

Fig. 31. Histogram of wear particle area for PTFE. Sliding conditions: same as in Fig. 29.

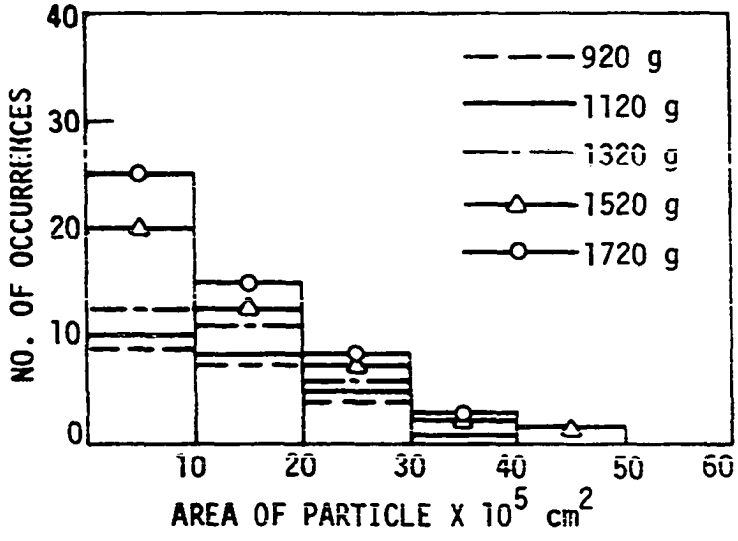

Fig. 32. Histogram of wear particle area for polypropylene. Sliding conditions: same as in Fig. 29.

Table 4. Surface area range for polymer wear particles.

Material	Area x 10^5 cm^2
PTFE	10-70
High density polyethylene	5-25
Polyoxymethylene	5-25
Polypropylene	5-25

Figure 33(a,b). As the sliding motion continues, the contacting asperities pass and the substrate of the softer material affected by this complex loading process undergoes elastic recovery. It is this recovery that is responsible for the formation of a wear particle that resembles a flattened ellipsoid, as shown in Figure 33(c). In order that a wear particle may be formed (by separation from the parent material), the elastic strain energy due to recovery in the unloaded condition must be equal to or greater than the surface energy of the particle (40), that is:

$$E_e \geq E_s \tag{55}$$

where E_e and E_s denote the elastic strain energy of the junction and surface energy of the particle, respectively. For a flattened ellipsoid, the elastic strain energy is given by:

$$E_e = \frac{1}{2} \frac{p_o^2}{E} \cdot V_p \tag{56}$$

where

p_o = normal stress on the junction

E = Young's modulus of elasticity of the particle material

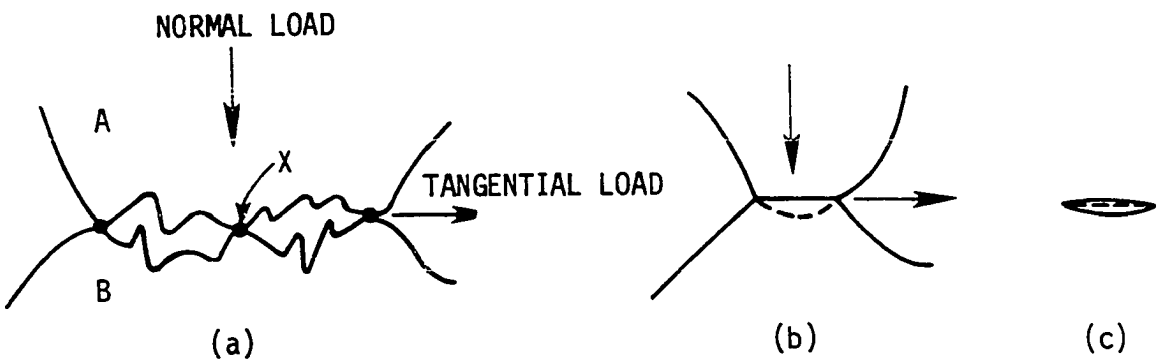

Fig. 33. Schematic illustration of the model for wear particle formation;
(a) adhesive junction due to contact between two asperities,
(b) shape of a potential wear particle at x in loaded conditions,
(c) shape of the wear particle due to recovery of junction in (b).

V_p = volume of flattened ellipsoid

$= \frac{\pi}{6}$ ABC (40, 41)

A and B, being the major and minor axes of the elliptical particle surface; and C, the thickness of wear particle.

The normal stress and shear stress acting on the junction give rise to the junction growth phenomenon (81, 82), so that

$$p_0^2 + \alpha_1 s^2 = \sigma_y^2 \tag{57}$$

and $$s = \mu p_0 \tag{58}$$

where σ_y is the yield strength, s, the shear stress acting at the junction, and α_1 is a constant.

Combining Equations (57) and (58), the pressure may be expressed as:

$$p_0 = \frac{\sigma_y}{(1+\alpha_1 \mu^2)^{1/2}} \tag{59}$$

Equation (56) therefore becomes

$$E_e = \frac{\pi}{12} \cdot \frac{\sigma_y^2}{(1+\alpha_1 \mu^2)E} \text{ ABC} \tag{60}$$

The surface area A_s of a flattened ellipsoid may be approximately expressed as:

A_s = surface area of ellipse + perimeter of ellipse

x $\frac{1}{2}$ (thickness of ellipsoid)

$$= \pi\left[\frac{AB}{4} + \sqrt{\frac{A^2+B^2}{2}}\,\frac{1}{2}\,\frac{2}{3}C\right] \tag{61}$$

Considering that the formation of a wear particle requires separation along only half the surface of the ellipsoid, the total surface energy

required is given by:

$$E_s = 2\pi\gamma\left[\frac{AB}{4} + \sqrt{\frac{A^2+B^2}{2}} \cdot \frac{1}{3} C\right] \tag{62}$$

where γ is the surface energy of the particle material.

Thus, the criterion for wear particle formation in Equation (55) gives:

$$\frac{\pi}{12} \cdot \frac{\sigma_y^2}{(1+\alpha_1\mu^2)E} \cdot ABC \geq 2\pi\gamma\left[\frac{AB}{4} + \sqrt{\frac{A^2+B^2}{2}} \cdot \frac{1}{3} C\right]$$

or

$$C \geq \frac{\gamma AB}{\left[\frac{\sigma_y^2}{6(1+\alpha_1\mu^2)E} \cdot AB - \frac{4}{3}\gamma\sqrt{\frac{A^2+B^2}{2}}\right]} \tag{63}$$

It should be noted that the above equation is in terms of the material properties and the coefficient of friction, both of which depend upon the sliding conditions. As for the constant α_1, a value of 3 as suggested in the literature (81) is assumed.

The thickness of a wear particle of high density polyethylene was calculated taking the following data:

γ = 31 erg/cm^2

μ = 0.2, as measured for a sliding speed of 0.5 m/sec and 920 g load

E = 0.2x10^{10} dynes/cm^2

σ_y = 1.1x10^8 dynes/cm^2

where E and σ_y were determined on a similar material bought from Cadillac Plastics and Chemical Co., (83). It was found to be 3440 Å, which is merely a rough estimate, recognizing that the sliding conditions dictate the strain rate in the substrate, which in turn governs the mechanical

properties of the material. Since the exact dependency betwen the sliding speed and strain rate is not known, the material properties used in the above equation were assumed to have a low strain rate condition normally used in tension tests. It is further recognized that the coefficient of friction will change with sliding conditions, but for the variation of load used in particle size measurements (the sliding speed having been kept constant), no appreciable change in the coefficient of friction was observed. It is felt that the moderate increase in wear with load is due to the increase in the number of adhesive junctions, and not because of any marked change in the wear particle size.

The wear particle formed in the manner described above may either escape from the interface or be entrapped between the high points of the sliding surfaces. What happens to the particle actually depends on the location of the particle in the contact zone at the instant it is formed. If the wear particle is entrapped, another strong bond is likely to be formed between the steel surface and the loose wear particle because of the much higher surface energy of the steel material as compared to that of the polymers. As soon as the steel surface is covered with worn polymer particles, the bond will be established between the newly-formed polymer wear particle and the polymer layer deposited on the steel surface. This particle will be liberated from the steel surface only if the elastic strain energy stored in it becomes greater than or equal to the adhesional energy acting over the interface, that is

$$E_e \geq E_a \tag{64}$$

where E_a is the adhesional energy. When this particle is relieved from

the normal and shear stresses acting at the interface due to sliding motion, the adhesion at the interface will prevent the particle from contracting and there will be a residual stress of magnitude $\frac{\varepsilon\sigma_y}{(1+\alpha_1\mu^2)^{1/2}}$ where ε is the Poisson's ratio of the particle material. It gives

$$E_e = \frac{1}{2}\frac{\varepsilon^2\sigma_y^2}{(1+\alpha_1\mu^2)E}\frac{\pi}{6}ABC_1 \tag{65}$$

and

$$E_a = \pi W_{ab}\left[\frac{AB}{4} + \sqrt{\frac{A^2+B^2}{2}}\frac{1}{3}C_1\right] \tag{66}$$

where W_{ab} is the work of adhesion, which is equal to 2γ for identical materials and equal to the arithmetic average of the surface energies for incompatible materials.

Thus, the use of Equation (64) gives

$$C_1 \geq \frac{W_{ab}AB}{\left[\frac{\sigma_y^2\varepsilon^2}{3(1+\alpha_1\mu^2)E}\cdot AB - \frac{4}{3}W_{ab}\sqrt{\frac{A^2+B^2}{2}}\right]} \tag{67}$$

Taking the same values of the material properties and the coefficient of friction for high density polyethylene as used above, the thickness of the wear particle was estimated as 20640 Å, using a Poisson's ratio of 0.4 (84).

The thickness of the wear particles for other materials as well was calculated using Equations (63) and (67). These values are given in Table 5, where the lower value is obtained from Equation (63) and the higher value from Equation (67). This shows that the wear particle thickness may range in practice by a factor of about 6-12, depending upon

Table 5. Estimated thickness of polymer wear particles.

Material	Å
High density polyethylene	3440 - 20640
PTFE	5090 - 56560
polyoxymethylene	2580 - 28670
polypropylene	6880 - 76444

what really happens to the particle. It should be noted that if the wear particle bonds again with the polymer surface, the result is an agglomeration of the wear particle. This is commonly observed in practice. The thickness of the wear particles estimated here agrees with the values reported by Makinson and Tabor (23) and Briscoe et al. (31) for PTFE and high density polyethylene sliding against metal and glass surfaces.

The Equations (63) and (67) derived above are similar in form and basis to those reported earlier by Rabinowicz (40). These differ with respect to the following:

1. The shape of the wear particle is considered to be that of a flattened ellipsoid instead of a sphere.
2. The junction growth arising from the combined effect of the normal and tangential stresses is also considered.

4.5. The Wear Model for Polymer-Metal Sliding

4.5.1. Mechanism of Wear at Low Sliding Speeds

An examination of the transmission electron micrographs of the replicas obtained from the sliding surfaces of semicrystalline polymers, namely, PTFE, high density polyethylene, polyoxymethylene and polypropylene, revealed that sliding of the metallic indentor at a low speed of 0.002 m/sec produces thin polymer films. These were observed to bridge across the abrasion grooves, and seem to have been produced by drawing because of the applied stress due to frictional resistance in the direction of sliding. Since the films had a thickness of a few hundred Å and were highly oriented, it is believed that they were produced as a result of shearing across the amorphous region between lamellae, as shown in Figure 34(a), (28, 30).

Thin films were also found on the sliding surface of polycarbonate, which is an amorphous polymer, but they were highly fragmented. These films also exhibited a high degree of orientation in the direction of sliding; they were formed because of deformation at the sliding surface which may result in the shearing of nodules, the molecules of which were aligned in the direction of sliding. This mechanism has been described speculatively in Figure 34(b), where the molecules A, B and C in the nodule are aligned in the direction of sliding to become A', B', and C' after deformation, thereby creating a better order in their arrangement.

4.5.2. Mechanism of Wear at Medium Sliding Speeds

In the experiments performed at sliding speeds of 0.25 m/sec (in temperature measurements), 0.5 m/sec (in wear particle analysis) and 1.5

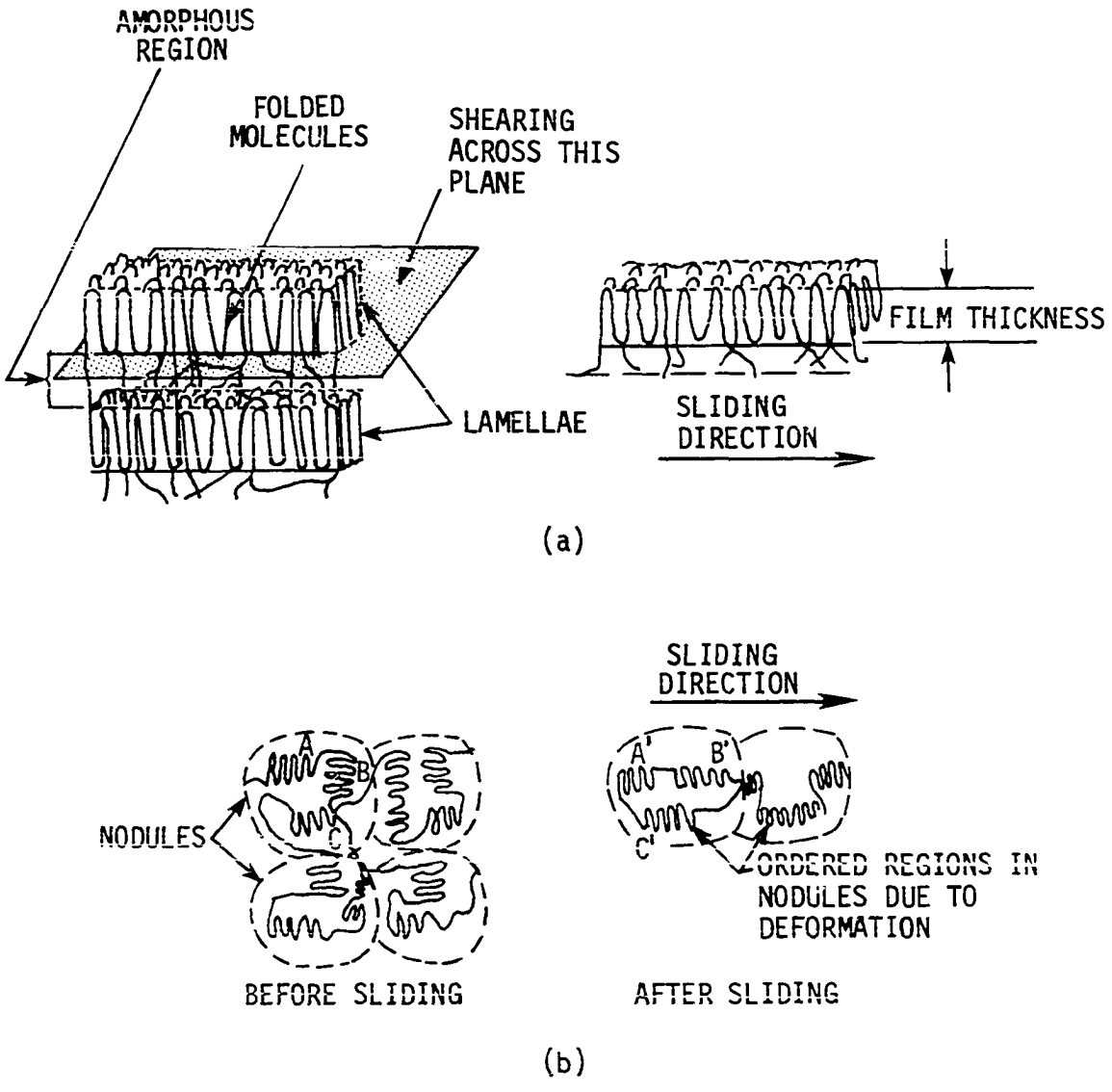

Fig. 34. Schematic of the proposed wear model; (a) crystalline polymers, (b) amorphous polymers.

m/sec (in scanning electron microscopy and DTA studies), lumpy wear particles were observed in case of PTFE, high density polyethylene and polyoxymethylene, in contrast to the thin films observed in low-speed sliding. These particles were assumed to be of a flattened ellipsoidal shape in the wear particle analysis. The thickness of such particles was estimated using the surface energy concept. Calculation showed the thickness to be several thousand Å to a few microns, depending upon whether a particle escaped from the interface or became locked between high points of the sliding surfaces. Makinson and Tabor (23) and Briscoe et al. (31) have also observed similar polymeric fragments several thousand Å thick, produced in the sliding of PTFE and high density polyethylene against metal and glass surfaces at speeds of 0.1 m/sec and higher. Since at high strain rates materials cease to exhibit the drawing phenomenon, the lumpy shape of the wear particles is due to characteristic deformation and fracture of the asperity junctions under these conditions.

4.5.3. Wear Failure at High Sliding Speeds

The temperature measurements showed that in the sliding speed range of 1.5-2.5 m/sec for polyethylene and 2.5-4 m/sec for polyoxymethylene, a transition from steady state to unsteady state condition takes place with the time of sliding. As a result of this transition the temperature rises leading finally to the failure of the polymeric pin by excessive wear. The temperature measurements, DTA and scanning electron microscopy studies led to the conclusion that the wear failure was due to the softening (melting) of the polymer rubbing surfaces.

There was no softening effect observed on the rubbing surface of PTFE. This is because its coefficient of friction, which is responsible

for the heat generated at the interface, was approximately one-fourth of that for the other two polymers. Furthermore, PTFE has a much higher melting point (327°C), and the measured temperature was always 240-280°C below it. Since temperature rise is directly proportional to sliding speed, softening is expected to occur at much higher speeds. Tanaka et al. (30) have reported the occurrence of softening on PTFE rubbing surface at a sliding speed of 19 m/sec.

5. CONCLUSIONS AND SUGGESTIONS

5.1. Conclusions

1. The temperature at the rubbing surface between a metal and polymer increased with time in the initial stages of sliding. This was followed by a steady state, during which the temperature remained constant. Depending upon the material and sliding conditions, the steady state was followed by an abrupt increase in temperature leading to failure due to excessive wear.

2. An equation was developed which considered steady state heat transfer, conduction of frictional heat in the radial direction, and heat loss by convection from both the periphery and sides of the disc. It showed good agreement between the predicted and measured values of temperature rise at the rubbing surface.

3. The transition from a steady state to an unsteady state sliding condition was found to occur in the sliding speed range of 1.5-2.5 m/sec for PTFE and high density polyethylene, and 2.5-4 m/sec for polyoxymethylene.

4. The failure of high density polyethylene and polyoxymethylene sliding members was due to thermal softening at the interface and excessive deflection of the projecting end of the pin, which created unstable sliding conditions. In contrast, the failure of PTFE was due to excessive wear and not to thermal softening. The latter was ruled out because the temperature measured at the rubbing surface was always 240-280°C below the melting point of the polymer.

5. Scanning electron microscopy revealed excessive material flow on the sliding surfaces of high density polyethylene and polyoxymethylene

at speeds higher than 1.5 m/sec. Such flow was not observed on the sliding surface of PTFE. At 1.5 m/sec sliding speed, softening was not observed at the polymer sliding surfaces, and lumpy fragments were found to have covered the sliding surfaces of the three polymers.

6. Transmission electron microscopy of replicas of the sliding surfaces of PTFE, high density polyethylene, polyoxymethylene and polypropylene revealed the presence of thin, continuous films stretched across abrasion grooves in the case of sliding at 0.002 m/sec. The films were highly oriented in the direction of sliding.

7. The rubbing surfaces in the case of sliding at speeds 0.25-1 m/sec were covered with lumpy wear particles resembling the shape of a flattened ellipsoid. From equations derived to estimate the thickness of wear particles, it was found that the thickness varied from 3440-20640 Å, 5090-56560 Å, 2580-28670 Å and 6880-76444 Å for high density polyethylene, PTFE, polyoxymethylene and polypropylene, respectively. The exact thickness depended on whether a particle escaped from the interface or was entrapped between high points of the sliding surfaces.

8. At a very low sliding speed of 0.002 m/sec, the mechanism of wear is by shearing and drawing of thin films for all the semi-crystalline polymers, whereas in the case of amorphous polycarbonate, the mechanism involved deformation and shearing of nodular regions. In the speed range of 0.5-1.5 m/sec, the drawing phenomenon ceased because of the strain rate dependency of the polymers; lumpy wear particles were produced as a result.

5.2. Suggestions for Future Work

1. It would be of interest to investigate the possibility of deriving an equation for temperature rise for the unsteady state condition at the sliding interface, considering phase transformation in the polymeric material.

2. It would also be desirable to verify the equation derived in this work for temperature rise considering the steady state heat transfer condition, by checking the predictions against experimental data obtained from the sliding between a metallic pin and a steel disc.

3. Polymers exhibit thermal softening when subjected to cyclic loading in fatigue. In a wear process too, the asperities undergo repetitive loading and unloading, which results in catastrophic failure due to softening. It would, therefore, be interesting to investigate whether a correspondence between fatigue and wear could be established.

4. Further investigations might include:

a) Development of a relationship for specifying the sliding conditions necessary to avoid catastrophic wear in polymers.

b) Development of a relationship between wear rate and wear particle characteristics, considering both the nature of the wear process and the surface characteristics of the sliding members.

c) Investigation of the fracture mechanism during sliding at medium speeds through examination of the replicas of worn polymer surfaces in a transmission electron microscope.

6. ACKNOWLEDGMENTS

The author wishes to express his sincere and profound gratitude to Professor Shyam Bahadur for his continued guidance, constant encouragement and proper counseling throughout the course of this work.

The author very much appreciates the advice and many important suggestions given by Professor Arthur E. Bergles, Chairman, Mechanical Engineering Department.

Appreciation is also extended to Professors John D. Verhoeven, Elmer Rosauer and Leo C. Peters for their willingness to act as members of the committee and for showing interest in the present study. The author would like to thank Professor G. A. Nariboli for providing guidance in the solutions of differential equations.

Thanks are also due to Mr. Hap Steed and Mr. Larry Couture for their assistance in the experimental work.

The funding and facilities of the Iowa State University Engineering Research Institute and the Mechanical Engineering Department are also appreciated.

The author is thankful to his wife Subhra and son Arindam for their inspiration and admirable patience during the course of this study.

The author wishes to thank Mr. V. K. Jain for following up the thesis through the final stages.

7. REFERENCES

1. Rabinowicz, E., and Tabor, D. "Metallic Transfer Between Sliding Metals: An Autoradiographic Study." Proc. Royal Society (London), Ser. A, 208 (1951), 455.

2. Burwell, J. T., and Strang, C. D. "Metallic Wear." Proc. Royal Society (London), Ser. A, 212 (1952), 470.

3. Archard, J. F. "Contact and Rubbing of Flat Surfaces." Journal of Applied Physics, 24 (1953, 981.

4. Archard, J. F., and Hirst, W. "The Wear of Metals Under Unlubricated Conditions." Proc. Royal Society (London), Ser. A, 236 (1956), 397.

5. Belyi, V. A., Sviridyonok, A. I., Smurugov, V. A., and Nevzorav, V. V. "Adhesive Wear of Polymers." In Wear of Materials - 1977, p. 526. Edited by W. A. Glaeser, K. C. Ludema and S. K. Rhee. New York: ASME, 1977.

6. Ratner, S. B. "Comparison of the Abrasion of Rubbers and Plastics." In Abrasion of Rubber, p.23. Edited by D. I. James. London: McLaren, 1967.

7. Ratner, S. B., Ferberova, I. I., Radyukevich, O. V., and Lure, E. G. "Connection Between the Wear Resistance of Plastics and Other Mechanical Properties." Soviet Plastics, 7 (1964), 37.

8. Ratner, S. B., and Lure, E. G. "Abrasion of Polymers as a Kinetic Thermo-Activation Process" and "Connection Between Abrasion and Thermo-Chemical Stability of Polymers." In Abrasion of Rubber, pp. 155 and 161. Edited by D. I. James. London: McLaren, 1967.

9. Lancaster, J. K. "Relationships Between the Wear of Polymers and Their Mechanical Properties." Proc. Institute of Mech. Engineers, 183 (1968-69), 98.

10. Lancaster, J. K. "Abrasive Wear of Polymers." Wear, 14 (1969), 223.

11. Vinogradov, G. V., Mustafaev, V. A., and Podlodsky, Yu.Ya. "A Study of Heavy Metal-to-Plastic Friction Duties and of the Wear of Hardened Steel in the Presence of Polymers." Wear, 8 (1965), 358.

12. Lancaster, J. K. "Friction and Wear." In Polymer Science, p. 989. Edited by A. D. Jenkins. New York: American Elsevier Co., 1972.

13. Aharoni, S. M. "Wear of Polymers by Roll Formation." Wear, 25 (1973), 309.

14. Suh, N. P. "The Delamination Theory of Wear." Wear, 25 (1973), 111.

15. Suh, N. P., Jahanmir, S., Abrahamson, E. P. and Turner, A. P. L. "Further Investigation of the Delamination Theory of Wear." Journal of Lubrication Technology, Trans. ASME, 96, Ser. F (1974), 631.

16. Giltrow, J. P. "A Relationship between Abrasive Wear and the Cohesive Energy of Materials." Wear, 15 (1970), 71.

17. Lontz, J. F. and Kumnick, M. C. "Wear Studies on Moldings of Polytetrafluoroethylene Resin, Considerations of Crystallinity and Graphite Content." ASLE Trans., 16 (1973), 276.

18. Warren, J. H., and Eiss, N. S. "Depth of Penetration as a Predictor of the Wear of Polymers on Hard, Rough Surfaces." In Wear of Materials - 1977, p. 494. Edited by W. A. Glaeser, K. C. Ludema and S. K. Rhee. New York: ASME, 1977.

19. Lewis, R. B. "Predicting the Wear of Sliding Plastic Surfaces." Mechanical Engineering, 86 (1964), 33.

20. Rhee, S. K. "Wear Equation for Polymers Sliding Against Metal Surfaces." Wear, 16 (1970), 431.

21. Pogosian, A. K. and Lambarian, N. A. "Estimation of Wear for Some Asbestos-Reinforced Friction Materials." In Wear of Materials - 1977, p. 547. Edited by W. A. Glaeser, K. C. Ludema and S. K. Rhee. New York: ASME, 1977.

22. Kar, M. K. and Bahadur, S. "Wear Equation for Unfilled and Filled Polyoxymethylene." Wear, 30 (1974), 337.

23. Makinson, K. R. and Tabor, D. "The Friction and Transfer of Polytetrafluoroethylene." Proc. Royal Society (London), Ser. A, 281 (1964), 49.

24. Pooley, C. M. and Tabor, D. "Friction and Molecular Structure: The Behavior of Some Thermoplastics." Proc. Royal Society (London), Ser. A, 329 (1972), 251.

25. Sviridyonok, A. I., Belyi, V. A., Smurugov, V. A. and Savkin, V. G. "A Study of Transfer in Frictional Interaction of Polymers." Wear, 25 (1973), 301.

26. Jain, V. K. and Bahadur, S. "Material Transfer in Polymer-Polymer Sliding." In Wear of Materials - 1977, p. 487. Edited by W. A. Glaeser, K. C. Ludema and S. K. Rhee. New York: ASME, 1977.

27. Bowers, R. C., Clinton, W. C. and Zisman, W. A. "Frictional Properties of Plastics." Modern Plastics, 321 (1954), 131.

28. Steijn, R. P. "The Sliding Surface of Polytetrafluoroethylene: An Investigation with the Electron Microscope." Wear, 12 (1968), 193.

29. Brainard, A. W. and Buckley, D. H. "Adhesion and Friction of PTFE in Contact with Metals as Studied by Augerspectroscopy, Field Ion and Scanning Electron Microscopy." Wear, 26 (1973), 75.

30. Tanaka, K., Uchiyama, Y., and Toyooka, S. "The Mechanism of Wear of Polytetrafluoroethylene." Wear, 23 (1973), 153.

31. Briscoe, B. J., Pogosian, A. K., and Tabor, D. "The Friction and Wear of High Density Polyethylene: The Action of Lead Oxide and Copper Oxide Fillers." Wear, 27 (1974), 19.

32. Tanaka, K. and Uchiyama, Y. "Friction, Wear and Surface Melting of Crystalline Polymers." In Advances in Polymer Friction and Wear, Vol. 5B, p. 499. Edited by L. H. Lee. New York: Plenum Press, 1974.

33. Tanaka, K. and Miyata, T. "Studies on the Friction and Transfer of Semicrystalline Polymers." Wear, 41 (1977), 383.

34. Antler, M. "Wear, Friction and Electrical Noise Phenomena in Severe Sliding Systems." ASLE Trans., 5 (1962), 297.

35. Wibberley, R. and Eyre, T. S. "The Dry Sliding Wear Characteristics of Copper, with and without 0.08% Silver." Wear, 13 (1969), 27.

36. Fehling, J. R. and Sarkar, N. K. "The Friction of Copper-Nickel and Iron-Sulfur Alloys in Air and Vacuum." Wear, 14 (1969), 33.

37. Kawamoto, M. and Okabayashi, K. "Wear of Cast Iron in Vacuum and the Frictional Hardened Layer." Wear, 17 (1971), 123.

38. Scott, D., Seifert, W. W., and Westcott, V. C. "The Particles of Wear." Scientific American, 230 (1974), 88.

39. Takagi, R. and Tsuya, Y. "Effect of Wear Particles on the Wear Rate of Unlubricated Sliding Metals." Wear, 5 (1962), 435.

40. Rabinowicz, E. Friction and Wear of Materials. New York: John Wiley & Sons, Inc., 1965.

41. Soda, N., Kimura, Y., and Tanaka, A. "Wear of Some F. C. C. Metals During Unlubricated Sliding, Part II: Effects of Normal Load, Sliding Velocity and Atmospheric Pressure on Wear Fragments." Wear, 35 (1975), 331.

42. Rabinowicz, E. "The Formation of Spherical Wear Particles." Wear, 42 (1977), 149.

43. Kimura, Y. "A Simple Method of Estimating the Mean Volume of a Wear Fragment." Journal of Japan Society of Lubrication Engineers, 17 (1972), 53.

44. Bahadur, S. and Stiglich, A. "Effect of Surface Roughness on the Wear of High Density Polyethylene." Technical Report, ERI Report 75102, Iowa State University, April 1975.

45. Vinogradov, G. V., Mustafaev, V. A. and Podlodsky, Yu. Ya. "A Study of Heavy Metal-to-Plastic Friction Duties and the Wear of Hardened Steel in the Presence of Polymers." Wear, 8 (1965), 358.

46. McLaren, K. G., and Tabor, D. "Friction of Polymers at Engineering Speeds: Influence of Speed, Temperature and Lubricants." Wear, 8 (1965), 79.

47. Bueche, A. M., and Flom, D. G. "Surface Friction and Dynamic Mechanical Properties of Polymers." Wear, 2 (1958/59), 168.

48. Watanabe, M., Karasawa, M., and Matsubana, K. "The Frictional Properties of Nylon." Wear, 12 (1968), 185.

49. Jaeger, J. C. "Moving Sources of Heat and Temperature at Sliding Contacts." Proc. Royal Society (N.S.W.), 56 (1942), 203.

50. Bowden, F. P. and Tabor, D. The Friction and Lubrication of Solids, Part I. Oxford: Clarendon Press, 1954.

51. Cook, N. H. and Bhusan, B. "Sliding Surface Interface Temperatures." Journal of Lubrication Technology, Trans. ASME, 95, Ser. F (1973), 59.

52. Archard, J. F. "The Temperature of Rubbing Surfaces," Wear, 2 (1958/59), 438.

53. Furey, M. J. "Surface Temperatures in Sliding Contact." ASLE Transactions, 7 (1964), 133.

54. Ling, F. F. "On Temperature Transients at Sliding Interface." Journal of Lubrication Technology, Trans. ASME, 91, Ser. F (1969), 397.

55. Kounas, P. S., Dimarogonas, A. D. and Sandor, G. N. "The Distribution of Friction Heat between a Stationary Pin and a Rotating Cylinder." Wear, 19 (1972), 415.

56. Harpavat, G. "Frictional Heating of a Uniform Finite Thickness Material Rubbing Against an Elastomer." In Advances in Polymer Friction and Wear, Vol. 5A, p. 205. Edited by L. H. Lee. New York: Plenum Press, 1974.

57. El-Sherbiny, M. and Newcomb, T. P. "The Temperature Distribution due to Frictional Heat Generated between a Stationary Cylinder and a Rotating Cylinder." Wear, 42 (1977), 23.

58. Eckert, E. R. G. and Drake, R. M. Analysis of Heat and Mass Transfer. New York: McGraw-Hill Book Co., 1972.

59. Anderson, J. T. and Saunders, O. A. "Convection from an Isolated Heated Horizontal Cylinder Rotating about its Axis." Proc. Royal Society (London), Ser. A, 27 (1953), 555.

60. Etemad, G. A. "Free Convection Heat Transfer from a Rotating Cylinder to Ambient Air, with Interferometric Study of Flow." Proc. Heat Transfer and Fluid Mechanics Institute, 7 (1954), 89.

61. Kays, W. M. and Bjorklund, I. S. "Heat Transfer from a Rotating Cylinder with and without Crossflow." Trans. ASME, 80 (1958), 70.

62. Richardson, P. D. and Saunders, O. A. "Studies of Flow and Heat Transfer Associated with a Rotating Disc." Journal of Mechanical Engineering Science, 5 (1963), 336.

63. Bahadur, S. "Mechanism of Dry Friction in Deformation Processing of Polymers." ERI Project 896-5, Final Report, Iowa State University, May 1973.

64. Tarr, P. R. "Methods for Connection to Revolving Thermocouples." NACA Research Memorandum, NACA RM E30J23a, (1951), 1.

65. Wunderlich, B. and Kashdan, W. H. "Thermodynamics of Crystalline Linear High Polymers. I: Comparison of the Melting Transitions of Solution and Melt Crystallized Polyethylene." Journal of Polymer Science, 1 (1961), 71.

66. Bunn, C. W. and Howells, E. R. "Structure of Molecules and Crystals of Fluorocarbons." Nature (London), 174 (1954), 549.

67. Speerschneider, C. J. and Li, Ch. H. "Some Observations on the Structure of Polytetrafluoroethylene." Journal of Applied Physics, 33 (1962), 1871.

68. Bunn, C. W. "The Crystal Structure of Long-Chain Normal Paraffin Hydrocarbons." "The 'Shape' of the > CH_2 Group." Transactions of the Faraday Society, 35 (1939), 482.

69. Uchida, T. and Tadokoro, H. "Structural Studies of Polyethers, IV. Structure Analysis of the Polyoxymethylene Molecule by Three-Dimensional Fourier Synthesis." Journal of Polymer Science, 5 (1967), 63.

70. Bahadur, S. "The Effect of Annealing on Mechanical Anisotropy of Cold Rolled Polyoxymethylene." SPE PACTEC 75, Las Vegas, 1975.

71. Natta, G. and Corrandini, P. "Structure and Properties of Isotactic Polypropylene." Nuovocimento, Suppl. to Vol. 15, 1 (1960), 40.

72. Binsberger, F. L. and DeLange, B. G. M. "Morphology of Polypropylene Crystallized from the Melt." Polymer, 9 (1968), 23.

73. Bahadur, S. "The Effect of Cold and Hot Extrusion on the Structure and Mechanical Properties of Polypropylene." Journal of Material Science, 10 (1975), 1425.

74. Neki, K. and Geil, P. H. "Morphology-Property Studies of Amorphous Polycarbonate." Journal of Macromolecular Science - Physics, B8 (1973), 295.

75. Geil, P. H. "Morphology of Amorphous Polymers." In Polymeric Materials, p. 119. Metals Park: American Society for Metals, 1974.

76. Yeh, G. S. Y. and Geil, P. H. "Strain-Induced Crystallization of Polyethylene Terephthalate." Journal of Macromolecular Science, B1 (1967), 251.

77. Fuller, C. S., Frosch, G. J., and Pape, N. R. "X-Ray Examination of Polyisobutylene." Journal of American Chemical Society, 62 (1940), 1905.

78. Andrews, E. H. "Crystalline Morphology in Thin Films of Natural Rubber. II. Crystallization under Strain." Proc. Royal Society (London), Ser. A, 277 (1964), 562.

79. Schoon, T. G. F. "Microstructure in Solid Polymers." British Polymer Journal, 2 (1970), 86.

80. Yeh, G. S. Y. and Luch, D. "Morphology of Strain-Induced Crystallization of Natural Rubber. I. Electron Microscopy of Uncrosslinked Thin Film." Journal of Applied Physics, 43 (1972), 4326.

81. Bowden, F. P. and Tabor, D. The Friction and Lubrication of Solids, Part II. Oxford: Clarendon Press, 1964.

82. Rowe, C. N. "Some Aspects of the Heat of Absorption in the Function of a Boundary Lubricant." ASLE Trans., 9 (1966), 100.

83. Bahadur, S. "Strain Hardening Equation and the Prediction of Tensile Strength of Rolled Polymers." Polymer Engineering and Science, 13 (1973), 266.

84. Van Krevelen, D. W. and Hoftyzer, P. J. Properties of Polymers Correlations with Chemical Structure. New York: Elsevier Publishing Co., 1972.

85. Beers, Y. Introduction to the Theory of Errors. Palo Alto: Addison-Wesley Co., 1962.

86. Thomas, G. Transmission Electron Microscopy of Metals. New York: John Wiley, 1966.

87. Siemen's Electron Microscope Instruction Manual. Berlin, Germany: Siemen and Co., 1962.

8. APPENDIX A: COMPUTER EVALUATION

Table A1. Computer evaluation of the modified Bessel function of the first kind, $I_n(\sigma R)$ (in this program a value of $\sigma R = 0.51$ has been used).

```
0001            DOUBLE PRECISION R(26),ARG,MMBSI0,MMBSI1
0002            IOPT=1
0003            ARG=0.51D0
0004            R(1)=MMBSI0(IOPT,ARG,IER)
0005            R(2)=MMBSI1(IOPT,ARG,IER)
0006            R(3)=R(1)-2.0*1.0/ARG*R(2)
0007            WRITE(6,1)R(1),R(2),R(3)
0008        1   FORMAT(1X,3F10.5,2X)
0009            DO20 I=4,26
0010            R(I)=R(I-2)-2.0*(I-2)/ARG*R(I-1)
0011            WRITE(6,11)R(I)
0012       20   CONTINUE
0013       11   FORMAT(2X,F15.5,3X)
0014            STOP
0015            END
```

```
1.06609   0.26338   0.03322
          0.00281
          0.00018
          0.00001
          0.00000
```

Table A2. Computer evaluation of the modified Bessel function of the second kind, $K_n(\sigma R)$ (in this program a value of $\sigma R = 0.51$ has been used).

```
0001            DOUBLE PRECISION R(26),MMBSK0,MMBSK1
0002            IOPT=1
0003            ARG=0.51D0
0004            R(1)=MMBSK0(IOPT,ARG,IER)
0005            R(2)=MMBSK1(IOPT,ARG,IER)
0006            R(3)=2.0*1.0/ARG*R(2)*R(1)
0007            WRITE(6,1)R(1),R(2),R(3)
0008        1   FORMAT(1X,3F10.5,2X)
0009            DO20 I=4,26
0010            R(I)=2.0*(I-2)/ARG*R(I-1)+R(I-2)
0011            WRITE(6,11)R(I)
0012       20   CONTINUE
0013       11   FORMAT(2X,F15.5,3X)
0014            STOP
0015            END
```

```
0.90806   1.61489   7.24096
        58.40676
       694.37935
     10950.63184
    215412.54906
   5079479.45785
```

9. APPENDIX B: ERROR ANALYSIS

The calculation of temperature rise involves two measured quantities, namely, the sliding speed (V), and coefficient of friction (μ). Any error in the measurement of these will contribute to an error in the calculated temperature. Since the sliding speed affects the coefficient of friction and vice versa, the errors are also related, making it a case of nonindependent error.

Let the error in the coefficient of friction and sliding speed be given by $d\mu$ and dV, respectively. Then the error in the calculated temperature rise may be expressed as (85):

$$dT = \frac{\partial T}{\partial \mu} d\mu + \frac{\partial T}{\partial V} dV \qquad \text{(B1)}$$

The steady state temperature rise at the rubbing surface is given by Equation (46):

$$T_D = \frac{\mu N V \gamma_1}{\pi J A' K_d} \cdot S$$

Differentiating the above, we get

$$\frac{\partial T_D}{\partial V} = \frac{\mu N \gamma_1 S}{\pi J A' K_d} \qquad \text{(B2)}$$

$$\frac{\partial T_D}{\partial \mu} = \frac{N V \gamma_1 S}{\pi J A' K_d} \qquad \text{(B3)}$$

Considering sliding motion under the following conditions:

$N = 1650$ g

$V = 1.5 \pm 0.075$ m/sec

$\mu = 0.3 \pm 0.03$ (measured) for polyoxymethylene pin and steel disc

(which assumes a variation of 5% in sliding speed and 10% in coefficient of friction), the total error dT was calculated.

Taking $J = 4.18 \times 10^7$ ergs/cal, $A' = 19.4$ cm^2, $R = 4.91$ cm, $K_d = 0.08$ cal/sec cm ^{o}C, and calculating $\gamma_1 = 0.988$ from Equation (48), we get from Equations (B2) and (B3):

$$\frac{\partial T_D}{\partial V} = 0.12$$

and

$$\frac{\partial T_D}{\partial \mu} = 59.4$$

Substituting these values in Equation (B1), we get

$$dT = 1.8\ ^{o}C.$$

10. APPENDIX C: CALCULATION OF INTERPLANAR DISTANCES AND DIFFRACTING PLANES

The equation used to calculate interplanar distance is (86):

$$\lambda S = r d_{spacing} \tag{C1}$$

where

λ = wavelength of electrons

S = camera constant or distance from specimen to film plane

= 54.5 cm (87)

r = radius of diffracting spot (on negative)

$d_{spacing}$ = interplanar distance

The wavelength λ was found to be 0.0418 Å (86) for an accelerating voltage of 80 kV used in the present work. Since PTFE has a hexagonal crystal structure, the following equation was used for the calculation of Miller indices of the diffracting planes:

$$\frac{1}{d^2_{spacing}} = \frac{4}{3}\left(\frac{h^2 + hK + k^2}{a^2}\right) + \frac{\ell^2}{c^2} \tag{C2}$$

where h, K and ℓ are the Miller indices of a plane.

The calculated results are given in Table C1.

Table C1. Interplanar distances and diffracting planes.

Material	Unit Cell Parameter	r, cm	$d_{spacing}$, Å	hkℓ
PTFE	a = 5.65 Å	1.2	1.94	(0010)
	c = 19.5 Å	1.45	1.62	(300)
		1.6	1.46	(306)
		1.8	1.29	(0015)